Title

Cell-Intrinsic CD38 Expression Sustains Exhausted CD8+ T Cells by Regulating Their Survival and Metabolism during Chronic Viral Infection



Journal

Journal of Virology, 97(4)

ISSN

0022-538X

Authors

DeRogatis, Julia M
Neubert, Emily N
Viramontes, Karla M
et al.

Publication Date

2023-04-27

DOI

10.1128/jvi.00225-23

Peer reviewed

AMERICAN SOCIETY FOR MICROBIOLOGY | Journal of Virology®

PATHOGENESIS AND IMMUNITY

# Cell-Intrinsic CD38 Expression Sustains Exhausted CD8$^+$ T Cells by Regulating Their Survival and Metabolism during Chronic Viral Infection

**Julia M. DeRogatis,[a] Emily N. Neubert,[a,b] Karla M. Viramontes,[a] Monique L. Henriquez,[a] Dequina A. Nicholas,[a] Roberto Tinoco[a,b]**

[a]Department of Molecular Biology and Biochemistry, School of Biological Sciences, University of California Irvine, Irvine, California, USA
[b]Center for Virus Research, University of California Irvine, Irvine, California, USA

**ABSTRACT** Acute and chronic viral infections result in the differentiation of effector and exhausted T cells with functional and phenotypic differences that dictate whether the infection is cleared or progresses to chronicity. High CD38 expression has been observed on CD8$^+$ T cells across various viral infections and tumors in patients, suggesting an important regulatory function for CD38 on responding T cells. Here, we show that CD38 expression was increased and sustained on exhausted CD8$^+$ T cells following chronic lymphocytic choriomeningitis virus (LCMV) infection, with lower levels observed on T cells from acute LCMV infection. We uncovered a cell-intrinsic role for CD38 expression in regulating the survival of effector and exhausted CD8$^+$ T cells. We observed increased proliferation and function of *Cd38*$^{-/-}$ CD8$^+$ progenitor exhausted T cells compared to those of wild-type (WT) cells. Furthermore, decreased oxidative phosphorylation and glycolytic potential were observed in *Cd38*$^{-/-}$ CD8$^+$ T cells during chronic but not acute LCMV infection. Our studies reveal that CD38 has a dual cell-intrinsic function in CD8$^+$ T cells, where it decreases proliferation and function yet supports their survival and metabolism. These findings show that CD38 is not only a marker of T cell activation but also has regulatory functions on effector and exhausted CD8$^+$ T cells.

**IMPORTANCE** Our study shows how CD38 expression is regulated on CD8$^+$ T cells responding during acute and chronic viral infection. We observed higher CD38 levels on CD8$^+$ T cells during chronic viral infection compared to levels during acute viral infection. Deleting CD38 had an important cell-intrinsic function in ensuring the survival of virus-specific CD8$^+$ T cells throughout the course of viral infection. We found defective metabolism in *Cd38*$^{-/-}$ CD8$^+$ T cells arising during chronic infection and changes in their progenitor T cell phenotype. Our studies revealed a dual cell-intrinsic role for CD38 in limiting proliferation and granzyme B production in virus-specific exhausted T cells while also promoting their survival. These data highlight new avenues for research into the mechanisms through which CD38 regulates the survival and metabolism of CD8$^+$ T cell responses to viral infections.

**KEYWORDS** CD38, LCMV, T cell exhaustion, effector T cell, metabolism, CD8$^+$ T cell, chronic viral infection, T cells

CD38 is an ectoenzyme expressed on the surface of most innate and adaptive immune cells and is upregulated during T cell activation (1). Upon contact between antigen-presenting cells (APCs) and CD8$^+$ T cells *in vitro*, CD38 localizes to the immunological synapse where its enzymatic functions increase intracellular $Ca^{2+}$ signaling (2, 3). As an ectoenzyme, CD38 converts $NAD^+$ to ADP-ribose (ADPR), cyclic-ADPR (cADPR), and $NAADP^+$ (1, 4–6). CD38 enzymatic activity has numerous physiological impacts, as ADPR, cADPR, and $NAADP^+$ all regulate cytoplasmic $Ca^{2+}$ levels while $NAD^+$, which is consumed by CD38, is a modulator of cellular metabolism, stress response, and circadian

**Editor** Mark T. Heise, University of North Carolina at Chapel Hill



Address correspondence to Roberto Tinoco, rtinoco@uci.edu.

The authors declare no conflict of interest.

**Received** 14 February 2023
**Accepted** 19 March 2023
**Published** 11 April 2023

rhythms (1, 4). Additionally, CD38 acts as a receptor on the surface of T cells, the ligation of which can further increase T cell activation through Lck-mediated activation of MAP kinase and CD3$\zeta$ signaling pathways (7). CD38 continues to be of interest, as it is highly expressed on T cells during numerous viral infections and cancers (3). CD38 is a key indicator of T cell activation during viral infection, and CD38$^{hi}$ CD8$^+$ T cells have been detected in patients infected with hepatitis C virus (HCV), HIV, Dengue, H1N1 influenza A virus (IAV), H7N9, Ebola, and severe acute respiratory syndrome coronavirus 2 (SARS-CoV-2) (8–16). However, the functional role of CD38 in the antiviral T cell response remains to be fully investigated.

While CD38 is upregulated with T cell activation during chronic infection and cancer, it is known to promote immunosuppression. CD38 negatively regulates inflammatory responses through the CD38/CD203/CD73 axis by converting NAD$^+$ to adenosine (17, 18). Adenosine signaling through the adenosine A2A receptor (A2AR) on T cells diminishes effector T cell functions, resulting in a loss of tumor control (19). Further, upregulation of CD38 on tumor cells increases adenosine production and limits T cell proliferation and responses to PD-1/PD-L1 checkpoint blockade (20). However, adenosine-driven resistance to immunotherapy can be overcome by the dual blockade of A2AR and PD-1, which enhances tumor-infiltrating CD8$^+$ T cell gamma interferon (IFN-$\gamma$) and granzyme B production (21).

Recently, there has been increased interest regarding the role of CD38 in T cell exhaustion, as CD38 expression was found to mark terminally exhausted T cells in tumors (22). Prolonged T cell receptor (TCR) stimulation, as in the case of chronic viral infections and cancer, leads T cells toward a dysfunctional state known as T cell exhaustion (23, 24). Exhausted T cells can differentiate into the following two distinct populations: progenitor exhausted T cells (Tpex) and terminally exhausted T cells (Tex) (25–27). The Tpex population is capable of self-renewal and can respond to immune checkpoint blockade (ICB), while the Tex population retains some effector functions but is short-lived and unresponsive to ICB. Delineating these populations is of clinical interest, as patient response to ICB can be driven by the presence or absence of Tpex and Tex cells. CD38, along with CD101, has emerged as a marker for the CD8$^+$ Tex population, which has a fixed epigenetic chromatin state that prevents these cells from regaining effector functions (22). Further, resistance to PD-1 ICB is driven by a population of suboptimally primed, dysfunctional PD-1$^+$ CD38$^{hi}$ CD8$^+$ T cells (28).

While CD38 is an established marker of terminal T cell exhaustion, whether CD38 has a role in promoting exhaustion is still being investigated. In a murine melanoma model, both CD38 deletion and overexpression in antigen-specific CD8$^+$ T cells were not sufficient to alter the exhaustion phenotype of tumor-infiltrating lymphocytes (29). In the case of chronic viral infections, such as HIV, CD38 expression is correlated with disease severity (30). As patients develop AIDS, the frequency of CD38-expressing CD8$^+$ T cells increases and then declines with antiretroviral treatment (31–33). However, the impact of CD38 expression on the phenotype and function of exhausted T cells in chronic viral infection is currently unknown (30). In this study, we used acute Armstrong (Arm) and chronic Clone 13 (Cl13) lymphocytic choriomeningitis virus (LCMV) to investigate the cell-intrinsic role of CD38 on virus-specific T cells during acute and chronic infection. In a cotransfer model of virus-specific wild-type (WT) and *Cd38*$^{-/-}$ P14$^+$ CD8$^+$ T cells, we show that *Cd38*$^{-/-}$ P14$^+$ CD8$^+$ T cells had decreased survival in both acute and chronic infection. We show that CD38 expression maintained transferred P14$^+$ Tpex and Tex populations in Cl13-infected mice but also restrained proliferation and granzyme B production in Tpex cells. We found that CD38 did not alter oxidative phosphorylation and glycolysis of adoptively transferred effector T cells generated during Arm infection, but exhausted *Cd38*$^{-/-}$ P14$^+$ T cells showed reduced metabolic function in both pathways. Taken together, our study shows that CD38 is an important regulator of virus-specific CD8$^+$ T cell survival in both acute and chronic infection. Our work presents an interesting paradigm for CD38 on CD8$^+$ Tpex cells, in which CD38 hinders their proliferation and granzyme B production but also ensures their survival.

## RESULTS

**CD38 expression is upregulated on exhausted CD8$^+$ T cells during chronic viral infection.** To assess how CD38 is regulated during acute and chronic viral infections, we infected WT mice with either LCMV Arm or Cl13 and measured PD-1 and CD38 expression on virus-specific T cells over the course of infection. Consistent with previous studies, PD-1 was highly expressed on LCMV major histocompatibility complex (MHC) class I tetramer$^+$ CD8$^+$ T cells early in chronic Cl13 infection and remained higher than acute infection, albeit to a lower level, over the course of infection (Fig. 1A). While PD-1 was also expressed during acute Arm infection, it remained significantly lower on virus-specific T cells when compared to Cl13 (Fig. 1A). As with PD-1, CD38 was also highly upregulated on LCMV MHC class I tetramer$^+$ CD8$^+$ T cells from Cl13-infected mice, peaking at 17 days postinfection (dpi) and remaining elevated throughout infection (Fig. 1B). CD38 was also upregulated on tetramer$^+$ CD8$^+$ T cells during Arm infection; however, levels were significantly lower compared to Cl13 infection. We next determined whether cells upregulate PD-1 and CD38 together during infection (Fig. 1C). In Cl13-infected mice, the majority of LCMV MHC class I tetramer$^+$ CD8$^+$ T cells coexpressed PD-1 and CD38 (Fig. 1C). In contrast, acutely infected mice had low frequencies of PD-1$^+$ CD38$^+$ tetramer$^+$ CD8$^+$ T cells (Fig. 1C). Next, we examined the regulation of CD38 during chronic viral infection in patients, using a previously published data set (GEO accession number GSE150345) (34). We analyzed HCV-specific CD8$^+$ T cell *CD38* expression in patients both during chronic HCV (cHCV) infection and after these patients received direct-acting antiviral (DAA) treatment that cured their infection. In data collected from three separate patients, *CD38* expression was high during cHCV infection, and levels decreased when these patients were cured from persistent infection (Fig. 1D). These findings showed that CD38 is expressed on virus-specific CD8$^+$ T cells during acute and chronic viral infection, but high expression is sustained on exhausted CD8$^+$ T cells.

**Cell-intrinsic CD38 expression supports the survival of virus-specific CD8$^+$ T cells during acute and chronic viral infection.** Since we saw CD38 expression on T cells during LCMV infection, we evaluated the cell-intrinsic role of CD38 in CD8$^+$ T cells during acute and chronic viral infection. We coinjected small numbers ($1 \times 10^3$ cells/each) of WT and *Cd38*$^{-/-}$ P14$^+$ T cell receptor (TCR) transgenic CD8$^+$ T cells specific for LCMV peptide $GP_{33–41}$ into WT mice (Fig. 2A). WT host mice (CD45.2$^+$) received WT P14$^+$ (CD45.1$^+$) and *Cd38*$^{-/-}$ P14$^+$ (CD45.1$^+$ CD45.2$^+$) T cells at a 1:1 ratio, and 1 day later were infected with LCMV Arm or Cl13. At 8 days post Arm infection, the frequencies and numbers of *Cd38*$^{-/-}$ P14$^+$ T cells in the spleen were significantly lower than WT P14$^+$ T cells (Fig. 2B to D). Over the course of infection, this phenotype persisted, with *Cd38*$^{-/-}$ P14$^+$ T cells present at lower frequencies and numbers out to 30 dpi (Fig. 2B, E, and F). *Cd38*$^{-/-}$ P14$^+$ T cells were also present at lower levels than WT P14$^+$ T cells in the blood at 8 and 30 dpi (see Fig. S1A and B in the supplemental material) and trended toward lower levels in the lymph nodes (Fig. S1B). Since lower frequencies of *Cd38*$^{-/-}$ P14$^+$ T cells were observed, we next investigated the survival of the cotransferred cells. At day 6 post Arm infection, *Cd38*$^{-/-}$ P14$^+$ T cells had significantly decreased frequencies of cleaved caspase-3$^+$ apoptotic cells (Fig. 2G). However, by 8 dpi and continuing to 30 dpi, this trend had reversed and *Cd38*$^{-/-}$ P14$^+$ T cells showed significantly increased frequencies of caspase-3$^+$ apoptotic cells (Fig. 2G).

Next, we investigated the role of CD38 in virus-specific T cells during chronic infection, using the same cotransfer setup described above. Adoptively transferred *Cd38*$^{-/-}$ P14$^+$ T cells were present at similar frequencies to WT P14$^+$ T cells at 8 dpi in the spleen and then dropped to significantly lower frequencies over the course of Cl13 infection (Fig. 2H, I, and K). This was true of the number of *Cd38*$^{-/-}$ P14$^+$ T cells as well, which were present at similar numbers to WT P14$^+$ T cells at 8 dpi (Fig. 2J) and then significantly lower numbers at 30 dpi (Fig. 2L). *Cd38*$^{-/-}$ P14$^+$ T cells were present at lower levels than WT P14$^+$ T cells in the blood at 8 dpi (Fig. S1C) and similar levels to WT P14$^+$ T cells in the blood and lymph nodes at 30 dpi (Fig. S1D). When apoptosis of adoptively transferred subsets was analyzed, *Cd38*$^{-/-}$ P14$^+$ T cells initially had reduced caspase-3$^+$ frequencies at 6 and 8 dpi, and then significantly higher frequencies of

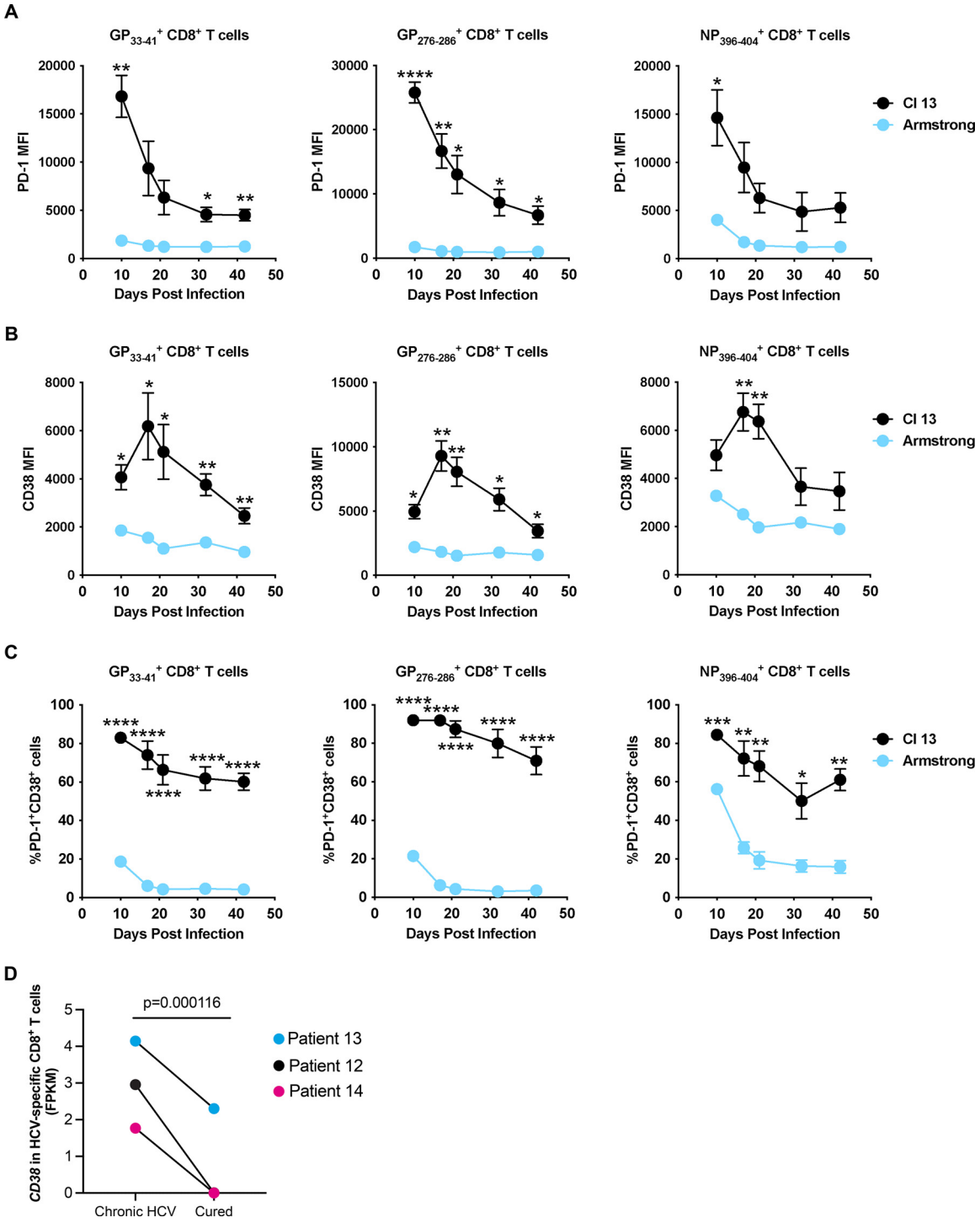


**FIG 1** CD38 expression and coregulation with PD-1 during acute and chronic infection. WT mice were infected with $2 \times 10^5$ PFU LCMV Armstrong i.p. or $2 \times 10^6$ PFU LCMV Cl13 i.v. (A) Geometric mean fluorescence intensity (MFI) of PD-1 on $GP_{33-41}$, $GP_{276-286}$, and $NP_{396-404}$ tetramer-specific CD8$^+$ T cells in blood of Arm- or Cl13-infected mice. (B) Geometric mean fluorescence intensity (MFI) of CD38 on $GP_{33-41}$, $GP_{276-286}$, and $NP_{396-404}$ tetramer-specific CD8$^+$ T cells in blood of Arm- or Cl13-infected mice. (C) Frequency of PD-1$^+$ CD38$^+$ $GP_{33-41}$, $GP_{276-286}$, and $NP_{396-404}$ tetramer-specific CD8$^+$ T cells in blood of Arm- or Cl13-infected mice. Virus-specific CD8$^+$ T cells were isolated from patients with hepatitis C infection, and low-input RNA-sequencing was performed by Hensel et al., 2021 (34) (GEO accession number GSE150345). (D) This data was used to graph the average normalized *CD38* expression in human HCV-specific CD8$^+$ T cells both during cHCV infection and after direct-acting antiviral (DAA) cure. Significance was assessed by differential analysis with multifactor design of paired samples using DESeq2. Data are representative of 3 independent experiments with ≥5 mice per group. Data show mean ± SEM. *, $P \leq 0.05$; ***, $P \leq 0.001$; ****, $P \leq 0.0001$ by multiple unpaired *t* test.

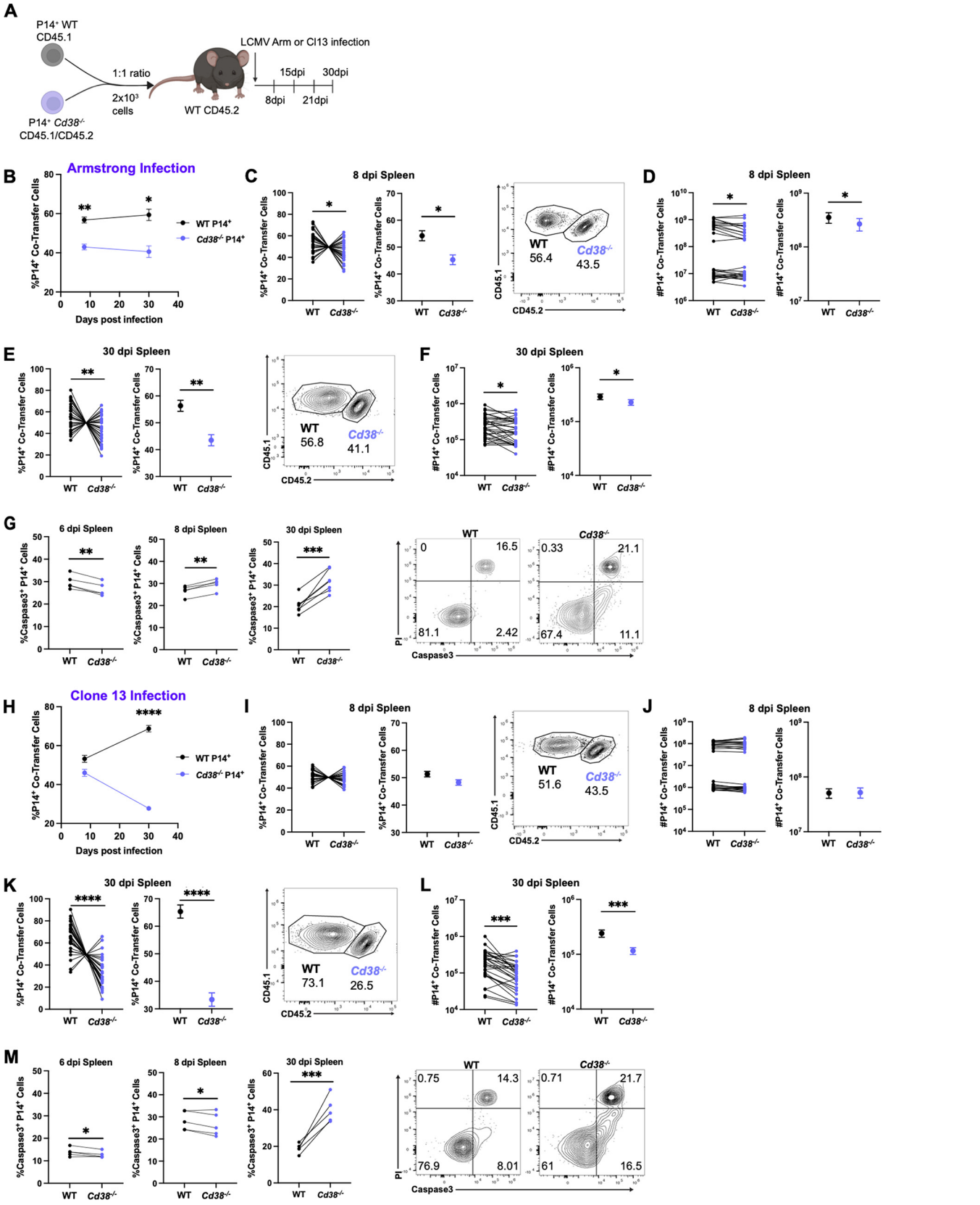


**FIG 2** Cell-intrinsic kinetics and survival of WT and *Cd38*$^{-/-}$ P14$^+$ T cells during acute and chronic LCMV infection. (A) WT and *Cd38*$^{-/-}$ P14$^+$ CD8$^+$ T cells were transferred at a 1:1 ratio (1 × 10$^3$ each) into WT naive mice, followed by LCMV Arm or Cl13 infection a day later. (B) Ratio of cotransferred WT and *Cd38*$^{-/-}$ P14$^+$ T cells in the spleen at 8 and 30 dpi in Arm-infected mice. (C) Individual ratios (left) and averaged

(Continued on next page)

caspase-3$^+$ apoptotic cells than WT P14$^+$ T cells at 30 dpi (Fig. 2M). Because we saw a reduction of *Cd38*$^{-/-}$ P14$^+$ T cells at multiple time points during acute and chronic infection, we wondered how these cells faired in competition with WT P14$^+$ T cells in uninfected mice. When WT and *Cd38*$^{-/-}$ P14$^+$ populations were examined in lymph nodes and spleens 24 h after adoptive transfer, there was a significant decrease in the frequencies of *Cd38*$^{-/-}$ P14$^+$ T cells (Fig. S1E and F). These findings showed a cell-intrinsic role for CD38 both in promoting initial residence in uninfected mice as well as survival of CD8$^+$ T cells during acute and chronic viral infection.

***Cd38*$^{-/-}$ CD8$^+$ T cells are activated after acute and chronic LCMV infection.** Because we saw that CD38 deletion impacted the survival phenotype of CD8$^+$ T cells during LCMV infection, we wanted to examine whether loss of CD38 also impacted the effector phenotype of CD8$^+$ T cells at 8 days post Arm and Cl13 infection. WT P14$^+$ (CD45.1) and *Cd38*$^{-/-}$ P14$^+$ (CD45.1$^+$/CD45.2$^+$) cells were cotransferred in small numbers ($2 \times 10^3$) into mice at a 1:1 ratio, and 1 day later, mice were infected with LCMV Arm or Cl13. The frequency of cotransferred granzyme B$^+$ cells was increased in *Cd38*$^{-/-}$ P14$^+$ T cells (Fig. 3A), while proliferating Ki67$^+$ P14$^+$ cell frequencies were similar between WT and *Cd38*$^{-/-}$ P14$^+$ T cells at 8 days post Arm infection (Fig. 3B). We next evaluated inhibitory receptor expression in WT and *Cd38*$^{-/-}$ P14$^+$ T cells and observed low frequencies of PD-1$^+$ TIM-3$^+$ at 8 days post Arm infection, with a slight increase in *Cd38*$^{-/-}$ cells (Fig. 3C). CD39, a marker of antigen-specific T cell engagement and an ectoenzyme capable of converting ATP to adenosine, was also analyzed on transferred P14$^+$ T cells and observed to be present at significantly higher frequencies in *Cd38*$^{-/-}$ than in WT P14$^+$ T cells (Fig. 3D) (35). When cytokine production was investigated, we observed similar frequencies of IFN-$\gamma^+$ and a small but significant increase of IFN-$\gamma^+$ tumor necrosis factor alpha-positive (TNF-$\alpha^+$) *Cd38*$^{-/-}$ P14$^+$ T cells compared to that of WT at day 8 post Arm infection (see Fig. S2A in the supplemental material). At day 8 post Cl13 infection, *Cd38*$^{-/-}$ P14$^+$ T cells had a small but significant increase in granzyme B production (Fig. 3E) and similar frequencies of Ki67$^+$ cells (Fig. 3F) when compared to those of WT P14$^+$ T cells. At 8 dpi, most transferred cells were PD-1$^+$, with significantly more PD-1$^+$ TIM-3$^+$ *Cd38*$^{-/-}$ P14$^+$ T cells than WT (Fig. 3G). The frequency of CD39$^+$ cells was also higher in transferred *Cd38*$^{-/-}$ P14$^+$ T cells than in WT P14$^+$ T cells (Fig. 3H). Compared to Arm infection, overall cytokine production was lower at 8 days post Cl13 infection, although *Cd38*$^{-/-}$ P14$^+$ T cells had increased frequencies of IFN-$\gamma^+$ and IFN-$\gamma^+$ TNF-$\alpha^+$ cells compared to those of the WT (Fig. S2B). Together, these findings demonstrate that while CD38 deletion did not alter proliferation in cotransferred P14$^+$ CD8$^+$ T cells at 8 dpi, loss of CD38 did promote an increase in granzyme B$^+$, PD-1$^+$ TIM-3$^+$, and CD39$^+$ cells in both Arm and Cl13 infection.

***Cd38*$^{-/-}$ CD8$^+$ T cell proliferation is increased at late stages of Cl13 infection.** While we observed similar frequencies of Ki67$^+$ WT and *Cd38*$^{-/-}$ P14$^+$ T cells at 8 days post Arm and Cl13 infection, we wanted to examine whether any differences occurred at 30 dpi. WT P14$^+$ (CD45.1) and *Cd38*$^{-/-}$ P14$^+$ (CD45.1$^+$/CD45.2$^+$) cells were cotrans-

**FIG 2** Legend (Continued)
ratio (right) of cotransferred WT or *Cd38*$^{-/-}$ P14$^+$ T cells from six experiments at 8 dpi in the spleen of Arm-infected mice. Representative FACS plots of cotransferred WT or *Cd38*$^{-/-}$ P14$^+$ T cells at 8 dpi in the spleen of Arm-infected mice. (D) Individual numbers (left) and averaged numbers (right) of cotransferred WT or *Cd38*$^{-/-}$ P14$^+$ T cells at 8 dpi in the spleen of Arm-infected mice. (E) Individual ratios (left) and averaged ratio (right) of cotransferred WT or *Cd38*$^{-/-}$ P14$^+$ T cells from six experiments at 30 dpi in the spleen of Arm-infected mice. Representative FACS plots (E), individual numbers (F, left) and averaged numbers (F, right) of cotransferred WT or *Cd38*$^{-/-}$ P14$^+$ T cells at 30 dpi in the spleen of Arm-infected mice. (G) Frequencies of caspase-3$^+$ apoptotic WT or *Cd38*$^{-/-}$ P14$^+$ T cells at 6, 8, and 30 dpi in the spleen of Arm-infected mice and representative FACS plots. (H) Ratio of cotransferred WT and *Cd38*$^{-/-}$ P14$^+$ T cells in the spleen at 8 and 30 dpi in Cl13-infected mice. (I) Individual ratios (left) and averaged ratio (right) of cotransferred WT or *Cd38*$^{-/-}$ P14$^+$ T cells from six experiments at 8 dpi in the spleen of Cl13-infected mice. Representative FACS plots of cotransferred WT or *Cd38*$^{-/-}$ P14$^+$ T cells at 8 dpi in the spleen of Cl13-infected mice. (J) Individual numbers (left) and averaged numbers (right) of cotransferred WT or *Cd38*$^{-/-}$ P14$^+$ T cells at 8 dpi in the spleen of Cl13-infected mice. (K) Individual ratios (left) and averaged ratio (right) of cotransferred WT or *Cd38*$^{-/-}$ P14$^+$ T cells from six experiments at 30 dpi in the spleen of Cl13-infected mice. Representative FACS plots (K), individual numbers (L, left), and averaged numbers (L, right) of cotransferred WT or *Cd38*$^{-/-}$ P14$^+$ T cells at 30 dpi in the spleen of Cl13-infected mice. (M) Frequency of caspase-3$^+$ apoptotic WT or *Cd38*$^{-/-}$ P14$^+$ T cells at 6, 8, and 30 dpi in the spleen of Cl13-infected mice and representative FACS plots. Data are representative of 6 independent experiments with ≥5 mice per group. Data show mean ± SEM. *, $P \leq 0.05$; ***, $P \leq 0.001$; ****, $P \leq 0.0001$ by paired *t* test.

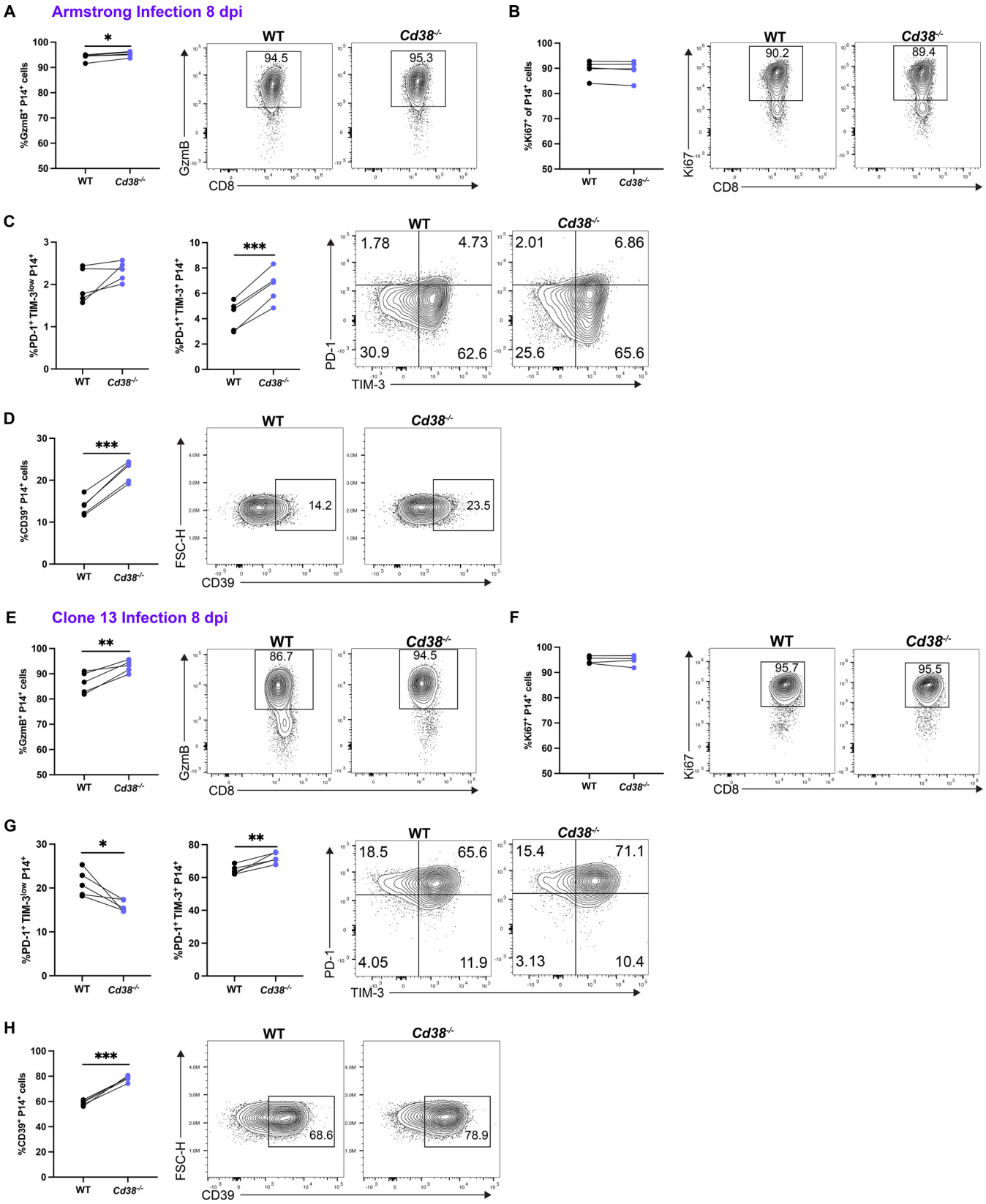


**FIG 3** Effector phenotype and function of WT and *Cd38*$^{-/-}$ P14$^+$ T cells at day 8 of acute or chronic LCMV infection. WT and *Cd38*$^{-/-}$ P14$^+$ CD8$^+$ T cells were transferred at a 1:1 ratio ($1 \times 10^3$ each) into WT naive mice, followed by LCMV Arm or Cl13 infection a day later. (A) Frequency and representative FACS plots of granzyme B$^+$ cotransferred WT and *Cd38*$^{-/-}$ P14$^+$ T cells at 8 dpi from spleens of Arm-infected mice. Frequency and representative FACS plots of Ki67$^+$ (B), PD-1$^+$ TIM-3$^{low}$ (C, left), PD-1$^+$ TIM-3$^+$ (C, right), and CD39$^+$ (D) cotransferred WT and *Cd38*$^{-/-}$ P14$^+$ T cells from spleens of Arm-infected

(Continued on next page)

ferred in small numbers ($2 \times 10^3$) into mice at a 1:1 ratio, and 1 day later, mice were infected with LCMV Arm or Cl13 and spleens were analyzed at 30 dpi. The frequency of granzyme B$^+$ and Ki67$^+$ cells were ~10% in both WT and *Cd38*$^{-/-}$ P14$^+$ T cells at 30 days post Arm infection (Fig. 4A and B). At 30 dpi, most WT and *Cd38*$^{-/-}$ P14$^+$ T cells were PD-1$^-$ TIM3$^-$ (Fig. 4C). The majority of WT and *Cd38*$^{-/-}$ P14$^+$ T cells at 30 dpi were IFN-$\gamma^+$ TNF-$\alpha^+$, with no differences in cytokine production observed (Fig. S2C). With Cl13 infection, we observed similar frequencies of granzyme B$^+$ cotransferred cells at 30 dpi (Fig. 4D). However, *Cd38*$^{-/-}$ P14$^+$ T cells had a significant increase in their proliferation as shown by the increase in Ki67$^+$ cells at 30 dpi (Fig. 4E). Most transferred cells were PD-1$^+$ TIM-3$^{low}$ at 30 dpi, and no differences were apparent in PD-1$^+$ TIM-3$^+$ populations between WT and *Cd38*$^{-/-}$ P14$^+$ T cells (Fig. 4F). Compared to Arm infection, there were decreased frequencies of IFN-$\gamma^+$ TNF-$\alpha^+$ transferred cells at day 30 post Cl13 infection; however, no differences were observed between WT and *Cd38*$^{-/-}$ P14$^+$ T cells (Fig. S2D). These findings showed that CD38 expression limited the proliferation of exhausted CD8$^+$ T cells while having minimal impact on cytokine production and inhibitory receptor expression.

**CD38 expression promotes the maintenance of Tpex and Tex subsets during chronic infection.** During chronic viral infection and cancer, exhausted T cells form two distinct populations, progenitor (Tpex) and terminal (Tex) exhausted T cells (27). Tpex cells are characterized by expression of the transcription factor TCF-1 and are capable of self-renewal and seeding of the Tex population, which retain better effector function but are short-lived (26, 27). To assess how CD38 may impact Tpex and Tex populations, we cotransferred small numbers ($2 \times 10^3$) of WT P14$^+$ and *Cd38*$^{-/-}$ P14$^+$ T cells into mice at a 1:1 ratio, infected mice with Cl13 1 day later, and then analyzed Tpex and Tex populations in the CD45.1$^+$ transferred cells in the spleen at 8 and 30 dpi. Although both WT and *Cd38*$^{-/-}$ P14$^+$ T cells differentiated into Tpex and Tex subsets at 8 dpi, the frequencies and numbers of *Cd38*$^{-/-}$ P14$^+$ Tpex were significantly decreased compared to WT (Fig. 5A). In contrast, the Tex population was composed of similar frequencies and numbers of WT and *Cd38*$^{-/-}$ P14$^+$ T cells at 8 dpi (Fig. 5B). On day 30 post Cl13 infection, the *Cd38*$^{-/-}$ P14$^+$ Tpex and Tex frequencies and numbers were significantly lower than WT P14$^+$ (Fig. 5C and D). When the frequencies of Tpex and Tex were tracked over the course of chronic infection, we found that *Cd38*$^{-/-}$ P14$^+$ T cells were more terminal than WT at 8 dpi (Fig. 5E). We next evaluated apoptosis in the transferred Tpex and Tex populations during infection and found that *Cd38*$^{-/-}$ P14$^+$ Tpex had more caspase-3$^+$ cells at 6 and 8 dpi and trended toward more at 30 dpi than WT P14$^+$ Tpex (Fig. 5F). *Cd38*$^{-/-}$ P14$^+$ Tex showed reduced caspase-3$^+$ cells at 6 and 8 dpi and increased caspase-3$^+$ cells at 30 dpi compared to that of WT P14$^+$ Tex (Fig. 5F). Further analysis of exhausted *Cd38*$^{-/-}$ P14$^+$ T cells showed increased frequencies of effector markers such CD69 and KLRG1 when compared to those of the WT (Fig. 5G and H) (36). Expression of the terminal marker 2B4$^+$ was similar in *Cd38*$^{-/-}$ and WT P14$^+$ T cells at 8 and 30 dpi (Fig. 5G and H). The frequencies of TCF-1$^+$ cells were reduced at 8 and 30 dpi with CD38 deletion (Fig. 5G and H). These findings showed that CD38 expression is important for the survival and maintenance of Tpex and Tex cells, as well as TCF-1 expression, over the course of chronic infection. Additionally, cells lacking CD38 show increased expression of markers associated with effector-like exhausted populations.

**CD38 negatively regulates the proliferation and function of progenitor exhausted CD8$^+$ T cells.** Because we saw an increase in surface markers indicative of effector-like exhausted cells, we next examined the impact of CD38 deletion on the effector functions of Tpex and Tex transferred cells. On day 8 post Cl13 infection, the

**FIG 3** Legend (Continued)
mice at 8 dpi. (E) Frequency and representative FACS plots of granzyme B$^+$ cotransferred WT and *Cd38*$^{-/-}$ P14$^+$ T cells from spleens of Cl13-infected mice at 8 dpi. Frequency and representative FACS plots of Ki67$^+$ (F), PD-1$^+$ TIM-3$^{low}$ (G, left), PD-1$^+$TIM-3$^+$ (G, right), and CD39$^+$ (H) cotransferred WT and *Cd38*$^{-/-}$ P14$^+$ T cells from spleens of Cl13-infected mice at 8 dpi. Data are representative of 3 independent experiments with ≥5 mice per group. Data show mean ± SEM. *, $P \leq 0.05$; ***, $P \leq 0.001$; ****, $P \leq 0.0001$ by paired *t* test.

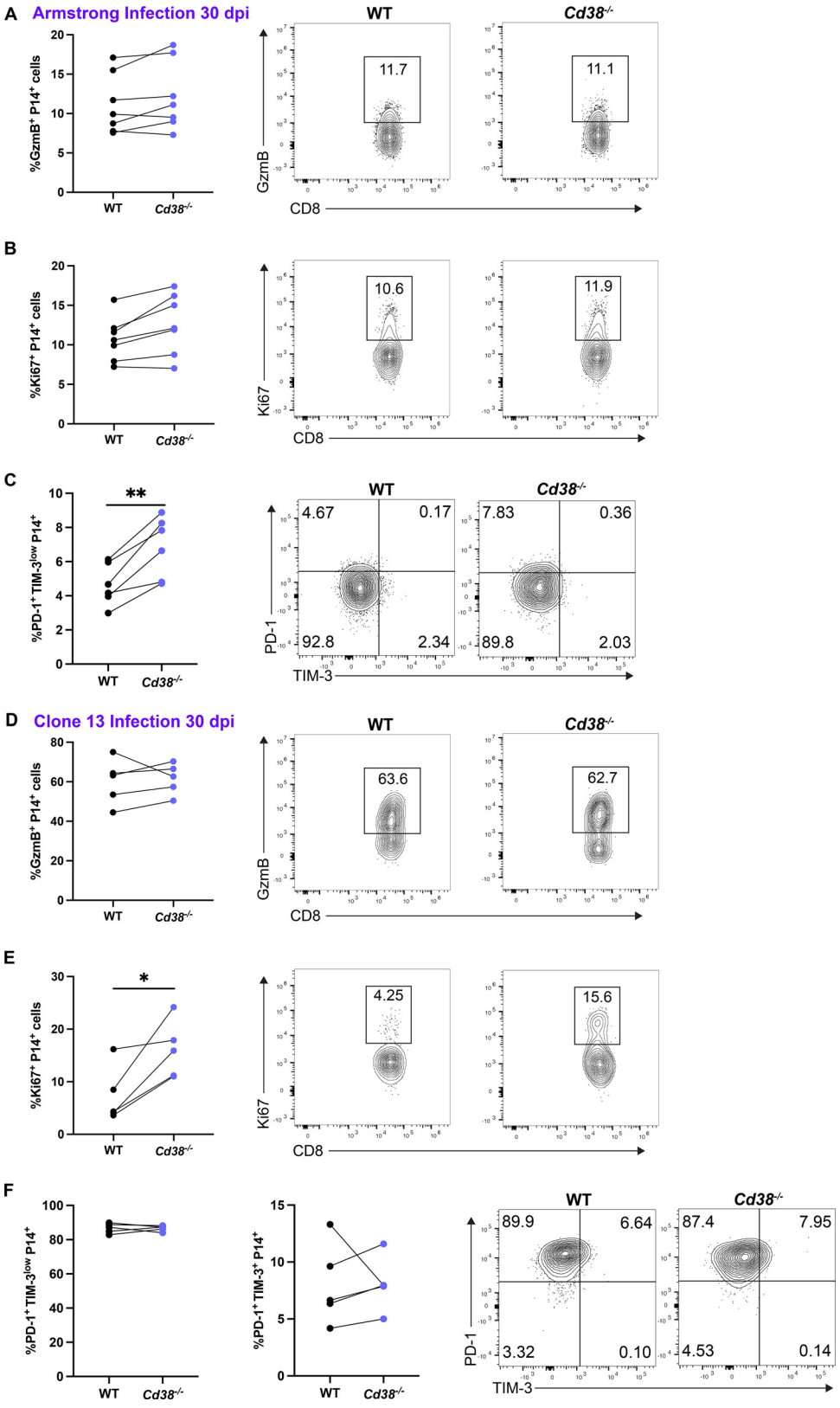


**FIG 4** Effector phenotype and function of WT and *Cd38*$^{-/-}$ P14$^+$ T cells at day 30 of acute or chronic LCMV. WT and *Cd38*$^{-/-}$ P14$^+$ CD8$^+$ T cells were transferred at a 1:1 ratio (1 $\times$ 10$^3$ each) into WT naive mice, followed by LCMV Arm or Cl13 infection a day later. (A) Frequency and representative FACS plots of granzyme B$^+$ cotransferred WT and *Cd38*$^{-/-}$ P14$^+$ T cells from spleens of Arm-infected mice at 30 dpi. Frequency and representative FACS plots of Ki67$^+$ (B) and PD-1$^+$TIM-3$^{low}$ (C) cotransferred WT and *Cd38*$^{-/-}$ P14$^+$ T cells from

(Continued on next page)

frequency of granzyme B$^+$ Tpex cells was significantly increased in *Cd38*$^{-/-}$ P14$^+$ T cells compared to that of the WT (Fig. 6A), whereas Ki67$^+$ cells were similar (Fig. 6B). *Cd38*$^{-/-}$ P14$^+$ Tex cells had a small but significant increase in granzyme B$^+$ cells and similar Ki67$^+$ cells compared to those of WT P14$^+$ Tex cells (Fig. 6C). At 30 dpi, *Cd38*$^{-/-}$ P14$^+$ Tpex had significantly more Granzyme B production and Ki67 than WT (Fig. 6D and E). *Cd38*$^{-/-}$ P14$^+$ Tex had similar Granzyme B and increased Ki67 production compared to WT P14$^+$ Tex (Fig. 6F). These findings showed that CD38 expression restrained granzyme B production and proliferation of Tpex cells during chronic infection.

**CD38 increased the metabolic fitness of CD8$^+$ T cells during chronic infection.** Since CD38 has enzymatic functions, we next examined whether metabolic changes occurred in *Cd38*$^{-/-}$ P14$^+$ T cells. To examine the impact of CD38 expression on mitochondrial respiration and glycolysis during LCMV infection, we carried out the Seahorse XF Cell Mito stress test on live-sorted WT and *Cd38*$^{-/-}$ P14$^+$ T cells from Arm or Cl13-infected mice at 8 dpi. CD38 deletion during Arm infection did not impact the P14$^+$ cell oxidative phosphorylation (Fig. 7A and B). Basal and maximal oxygen consumption rate (OCR) (a proxy for oxidative phosphorylation) and extracellular acidification rate (ECAR) (a proxy for glycolysis) were indistinguishable between WT and *Cd38*$^{-/-}$ P14$^+$ T cells from Arm-infected mice (Fig. 7C and D). The ratio of OCR/ECAR was also quantified to gain a relative measure of cellular preference for oxidative phosphorylation or glycolysis (Fig. 7E). At 8 days post Arm infection, CD38 deletion did not significantly impact the OCR/ECAR ratio. In contrast to Arm infection, CD38 deletion in P14$^+$ T cells from mice infected with Cl13 resulted in decreased oxidative phosphorylation and glycolysis (Fig. 7F and G). The basal and maximal OCR of *Cd38*$^{-/-}$ P14$^+$ T cells were decreased compared to those of WT P14$^+$ T cells from Cl13-infected mice (Fig. 7H). Basal and maximal ECAR levels were also significantly decreased with CD38 deletion (Fig. 7I). Basal and maximal OCR/ECAR ratios were similar between WT and *Cd38*$^{-/-}$ P14$^+$ T cells from Cl13-infected mice (Fig. 7J). Relative to Arm infection, the larger OCR/ECAR ratios in Cl13 samples demonstrated a preference for oxidative phosphorylation (Fig. 7J). These findings showed that cell intrinsic CD38 expression sustained the basal and maximal metabolic function of exhausted CD8$^+$ T cells during Cl13 infection.

## DISCUSSION

CD38 upregulation on activated T cells has been associated with response to infections (30). More recently, CD38 was found to mark terminal T cell dysfunction and has gained interest as a possible pharmacological target for the enhancement of T cell responses (22, 37). However, the functional role of CD38 on T cells in response to acute and chronic viral infection remains largely undefined. In this study, we used an adoptive cotransfer of *Cd38*$^{-/-}$ P14$^+$ and WT P14$^+$ CD8$^+$ T cells to investigate the cell-intrinsic role of CD38 on virus-specific T cells. We found that CD38 promotes the survival of CD8$^+$ T cells during LCMV infection. In an acute infection, proliferation and granzyme B production were not limited by CD38 expression. While CD38 expression seems to play a relatively minor role in shaping the effector response of CD8$^+$ T cells to acute infection, we found that CD38 is an important regulator of cell proliferation and granzyme B production, Tpex and Tex phenotype and maintenance, and metabolism during chronic infection.

During HIV infection, CD38 is upregulated on T cells and can serve as a marker of disease progression (32, 38, 39). In cases of H7N9 avian influenza, a larger population of CD38$^+$ HLA-DR$^+$ CD8$^+$ T cells are found in patients who succumb to flu (13). In both Dengue- and Ebola-infected patients, CD8$^+$ CD38$^+$ T cells are upregulated in febrile

**FIG 4** Legend (Continued)
spleens of Arm-infected mice at 30 dpi. (D) Frequency and representative FACS plots of granzyme B$^+$ cotransferred WT and *Cd38*$^{-/-}$ P14$^+$ T cells from spleens of Cl13-infected mice at 30 dpi. Frequency and representative FACS plots of Ki67$^+$ (E), PD-1$^+$ TIM-3$^{low}$ (F, left), and PD-1$^+$ TIM-3$^+$ (F, right) cotransferred WT and *Cd38*$^{-/-}$ P14$^+$ T cells from spleens of Cl13-infected mice at 30 dpi. Data are representative of 6 independent experiments with ≥4 mice per group. Data show mean ± SEM. *, $P \leq 0.05$; ***, $P \leq 0.001$; ****, $P \leq 0.0001$ by paired *t* test.

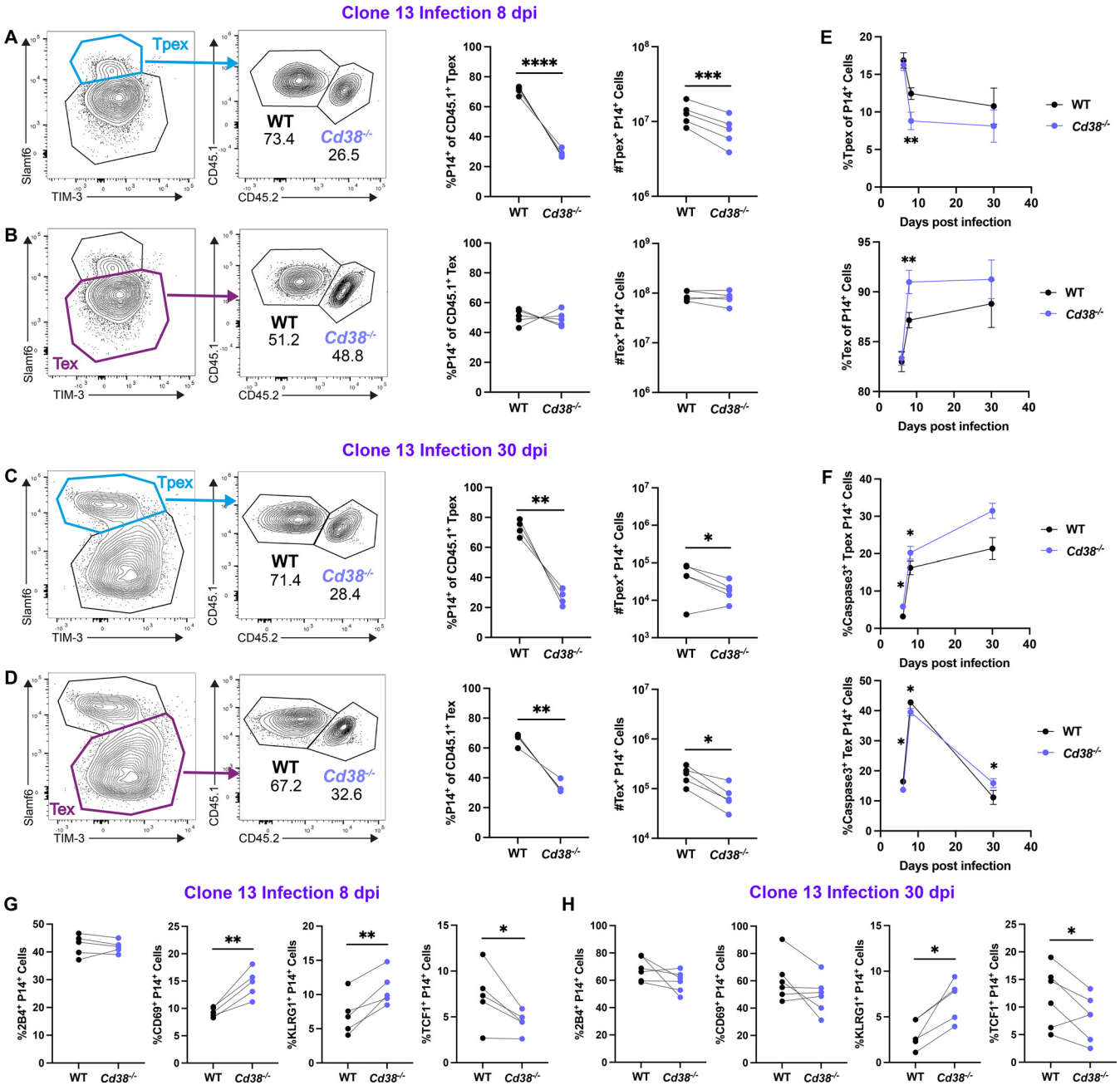


**FIG 5** Analysis of exhausted populations in WT and *Cd38*$^{-/-}$ P14$^+$ T cells during Cl13 infection. WT and *Cd38*$^{-/-}$ P14$^+$ CD8$^+$ T cells were transferred at a 1:1 ratio ($1 \times 10^3$ each) into WT naive mice, followed by LCMV Cl13 infection a day later. (A) Frequencies of WT or *Cd38*$^{-/-}$ P14$^+$ T cells of total cotransferred Tpex cells, representative FACS plots, and numbers of total Tpex at 8 dpi in spleen. (B) Frequencies of WT or *Cd38*$^{-/-}$ P14$^+$ T cells of total cotransferred Tex cells, representative FACS plots, and numbers of total Tex at 8 dpi in spleen. (C) Frequencies of WT or *Cd38*$^{-/-}$ P14$^+$ T cells of total cotransferred Tpex cells, representative FACS plots, and total numbers of Tpex at 30 dpi in spleen. (D) Frequencies of WT or *Cd38*$^{-/-}$ P14$^+$ CD8$^+$ T of total cotransferred Tex cells, representative FACS plots, and total numbers of Tex at 30 dpi in spleen. (E) Frequencies of cotransferred Tpex and Tex cells in the spleen over the course of Cl13 infection. (F) Frequencies of apoptotic caspase-3$^+$ cotransferred Tpex and Tex in the spleen over the course of Cl13 infection. Frequencies of 2B4$^+$, CD69$^+$, KLRG1$^+$ and TCF1$^+$ cotransfer cells at 8 dpi (G) and 30 dpi (H) in the spleen. Data are representative of 3 (8 dpi spleen), 6 (30 dpi spleen), or 2 (2B4 and CD69 expression) independent experiments with ≥4 mice per group. Data show mean ± SEM. *, $P \leq 0.05$; ***, $P \leq 0.001$; ****, $P \leq 0.0001$ by paired *t* test.

patients (11, 13, 40). In concurrence with these data, we found that CD38 levels were elevated on T cells during Arm and Cl13 infection, although to a much higher extent in Cl13. Our study and others have shown that CD38 is coexpressed with PD-1 and correlates with activation as well as exhaustion (13). As with PD-1, CD38 is expressed during activation in response to acute infection, and CD38 levels are elevated and sustained on exhausted T cells during chronic infection. This differential expression is a result of

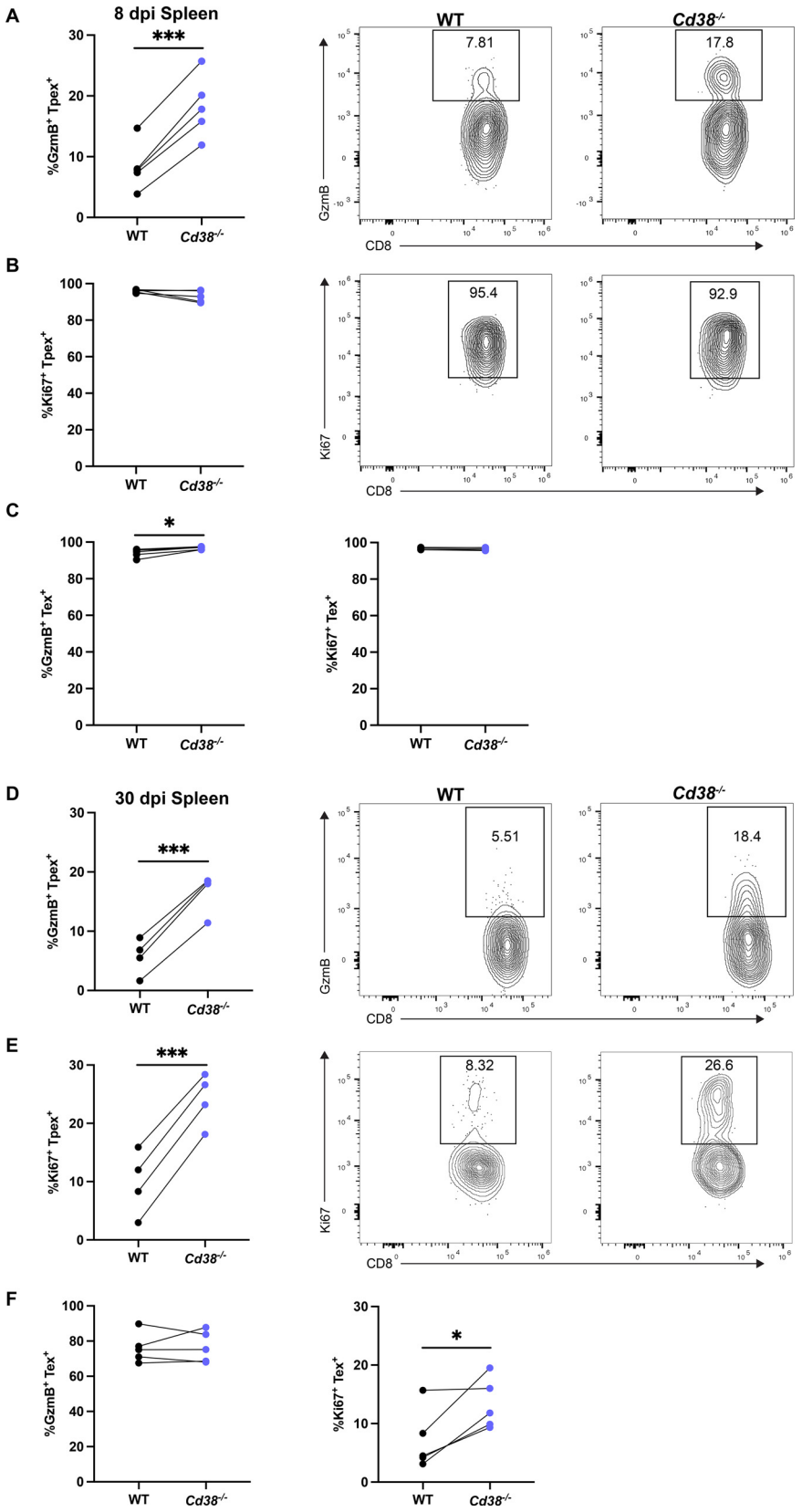


**FIG 6** *Cd38*$^{-/-}$ P14$^+$ Tpex and Tex cell phenotypes in Cl13 infection. WT and *Cd38*$^{-/-}$ P14$^+$ CD8$^+$ T cells were transferred at a 1:1 ratio (1 × 10$^3$ each) into WT naive mice, followed by LCMV Cl13 infection a day later. (A) Frequencies of granzyme B$^+$ WT or *Cd38*$^{-/-}$ Tpex cells at 8 dpi in spleen and

(Continued on next page)

divergent chromatin accessibility in T cells during acute and chronic infection (41). Regions of the *Pdcd1* locus become uniquely accessible at day 5 and onward during tumorigenesis and at day 8 postinfection and onward during chronic infection (22, 41, 42). Similarly, the *Cd38* locus is uniquely open in both virus and tumor-specific exhausted T cells (22, 43). The expression patterns and chromatin accessibility of CD38 make it a particularly good marker of chronic T cell stimulation and raises the question of how CD38 signaling may shape the phenotype of activated T cells. Interestingly, our analysis of the Hensel et al. (34) study showed that CD38 gene expression levels were high on CD8$^+$ T cells from patients with chronic HCV, but these were decreased when the same patients were cured from their infection, suggesting that CD38 expression may be linked to persistent TCR stimulation.

As an ectoenzyme, the immunosuppressive function of CD38 has been well established through its contribution in regulating extracellular adenosine levels. CD38, in conjunction with CD203a and CD73 enzymatic activities, converts extracellular NAD$^+$ to adenosine (17). In the tumor microenvironment, CD38-expressing tumor cells and myeloid-derived suppressor cells produce adenosine to limit cytotoxic T cell function through the adenosine receptor (20, 44, 45). Blocking the immunosuppressive adenosine pathway through targeting of the adenosine (A2A) receptor or CD73 has proven beneficial to antitumor T cell responses (21, 45, 46). While less is known about the cell-intrinsic role of CD38 on virus- or tumor-specific T cells, evidence suggests CD38 as a possible inhibitor of T cell function (11, 22, 28). We found that CD38 deletion did not impact cytokine production of CD8$^+$ T cells during Arm and Cl13 infection. While CD38 deletion did promote increased PD-1 and TIM-3 expression at 8 dpi, by 30 dpi the impact of deletion on inhibitory receptor expression was minimal. These findings are consistent with a recent study showing that overexpression or deletion of CD38 on tumor-specific T cells did not alter their exhaustion phenotype (29). CD73 is downstream of CD39, another ectoenzyme capable of initiating conversion of ATP to adenosine (47, 48). The limited impact of CD38 deletion on virus-specific T cells at 8 days post LCMV infection may be partially due to the redundancy of enzymatic functions of CD39, CD73, and CD203 in adenosine formation (17). This is relevant, as we saw an increase in CD39$^+$ cells in *Cd38*$^{-/-}$ P14$^+$ T cells. This indicates that CD38 deletion alone may not be enough to alter immunosuppressive adenosine signaling.

While effector functions were largely similar in cotransferred WT and *Cd38*$^{-/-}$ P14$^+$ CD8$^+$ T cells at 30 dpi, we discovered an important cell-intrinsic role for CD38 expression in the survival of virus-specific CD8$^+$ T cells. We found that adoptively transferred *Cd38*$^{-/-}$ P14$^+$ T cells were significantly decreased by day 30 post Arm and Cl13 infection due in part to increased apoptosis. Interestingly, when we performed cotransfers of naive *Cd38*$^{-/-}$ and WT P14$^+$ T cells into uninfected mice, cells lacking CD38 had diminished frequencies by 24 h. This indicated that CD38 may also play a cell-intrinsic role of homing of naive T cells. Our data indicate that *Cd38*$^{-/-}$ P14$^+$ T cells can expand in response to viral infection (as indicated by the similar frequencies in spleens of Cl13-infected mice at 8 dpi); however, these cells are unable to persist over the course of infection. A similar loss of adoptively transferred *Cd38*$^{-/-}$ tumor-specific T cells compared to WT was seen in tumors 14 days after transfer (29). Interestingly, the decreased frequency of *Cd38*$^{-/-}$ T cells was not attributed to apoptosis in the tumor model, whereas in the LCMV model, *Cd38*$^{-/-}$ P14$^+$ T cells had increased caspase-3 expression. Further research is needed to define the cell-intrinsic mechanism that drives the loss of

**FIG 6** Legend (Continued)
representative FACS plots. (B) Frequencies of Ki67$^+$ WT or *Cd38*$^{-/-}$ Tpex cells at 8 dpi in spleen and representative FACS plots. (C) Frequencies of granzyme B$^+$ and Ki67$^+$ cotransferred WT or *Cd38*$^{-/-}$ Tex P14$^+$ T cells in the spleen. (D) The 8 dpi frequencies of granzyme B$^+$ WT or *Cd38*$^{-/-}$ Tpex cells at 30 dpi in spleen and representative FACS plots. (E) Frequencies of Ki67$^+$ WT or *Cd38*$^{-/-}$ Tpex cells at 30 dpi in spleen and representative FACS plots. (F) The 30 dpi frequencies of granzyme B$^+$ and Ki67$^+$ cotransferred WT or *Cd38*$^{-/-}$ Tex P14$^+$ T cells in the spleen. Data are representative of 3 (8 dpi spleen) or 6 (30 dpi spleen) independent experiments with ≥4 mice per group. Data show mean ± SEM. *, $P \leq 0.05$; ***, $P \leq 0.001$; ****, $P \leq 0.0001$ by paired *t* test.

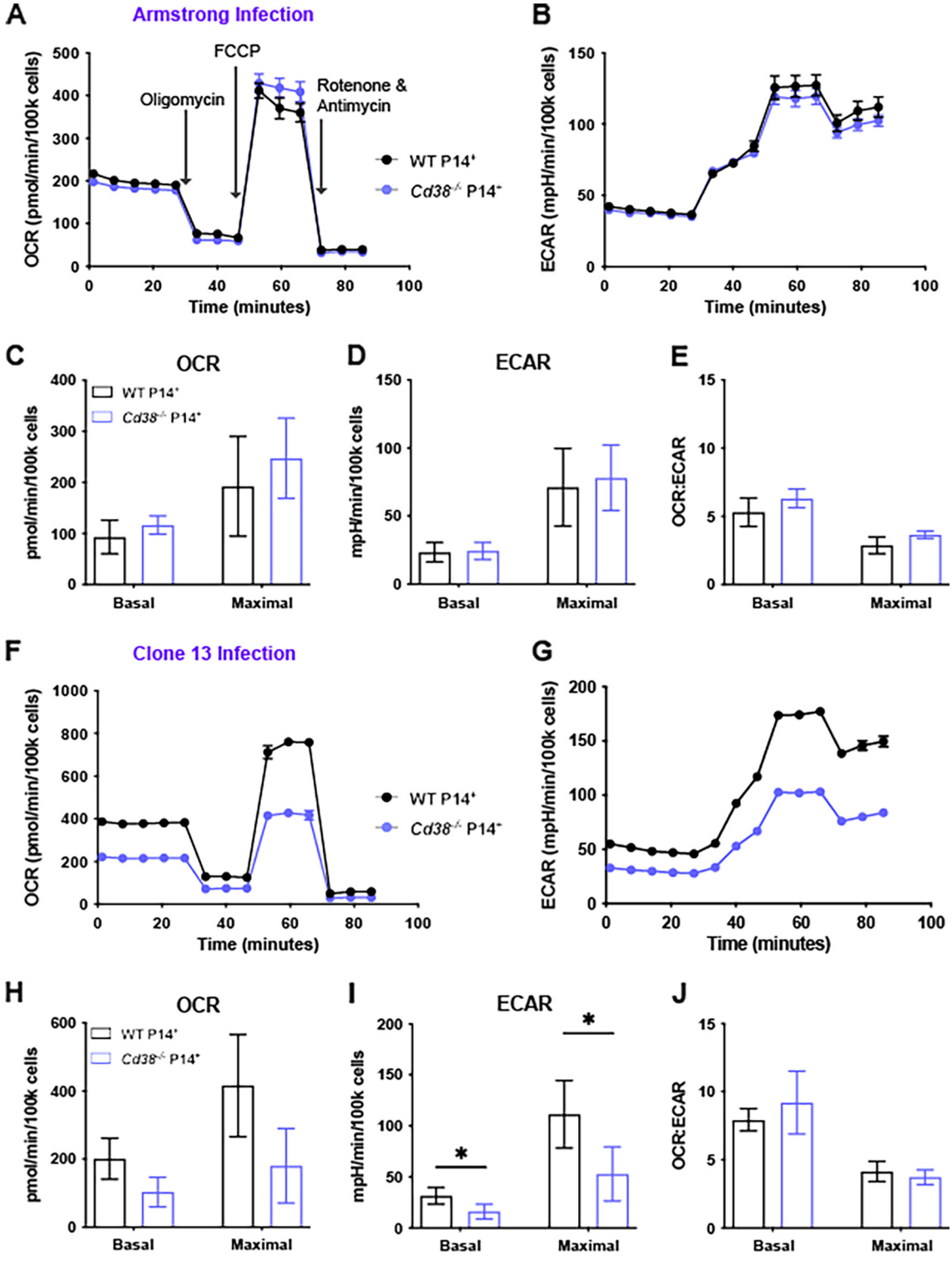


**FIG 7** Metabolism of *Cd38*$^{-/-}$ virus-specific CD8$^+$ T cells. WT and *Cd38*$^{-/-}$ P14$^+$ CD8$^+$ T cells were transferred at a 1:1 ratio ($1 \times 10^3$ each) into WT naive mice, followed by LCMV Arm or Cl13 infection a day later. Live WT and *Cd38*$^{-/-}$ P14$^+$ CD8$^+$ T cells were isolated from host mice at 8 dpi and a Seahorse XF Cell Mito stress test was performed. (A) Oxygen consumption rate (OCR) of live WT and *Cd38*$^{-/-}$ P14$^+$ T cells from Arm-infected mice at baseline and after addition of oligomycin, FCCP, and rotenone & antimycin A. (B) Extracellular acidification rate (ECAR) of live WT and *Cd38*$^{-/-}$ P14$^+$ T cells from Arm-infected mice at baseline and after addition of Mito stress test compounds. (C–E) Basal and maximal OCR and ECAR rates and quantified OCR/ECAR ratio for isolated WT and *Cd38*$^{-/-}$ P14$^+$ T cells from Arm-infected mice. (F, G) Seahorse XF Cell Mito stress test OCR and ECAR values from live WT and *Cd38*$^{-/-}$ P14$^+$ T cells isolated from Cl13-infected mice at 8 dpi. (H–J) Basal and maximal OCR and ECAR rates and quantified OCR/ECAR ratio for isolated WT and *Cd38*$^{-/-}$ P14$^+$ T cells from Cl13-infected mice. Seahorse data presented are median values of a representative biological replicate. Data are representative of 3 independent experiments with ≥5 mice per group for Arm and ≥15 mice for Cl13 infection. Data show mean ± SEM. *, $P \leq 0.05$; ***, $P \leq 0.001$; ****, $P \leq 0.0001$ by paired *t* test.

*Cd38*$^{-/-}$ T cells in uninfected mice and in tumor models. TCR signaling has been shown to regulate CD38, and a corresponding role for CD38 in promoting survival could explain its persistent expression on memory and exhausted T cells in mice and in patients with viral infections and autoimmune disorders (39, 49–52). Given its upregulation on activated and memory T cells, and considering we show that transferred *Cd38*$^{-/-}$ P14$^+$ T cells undergo significantly more apoptosis than WT P14$^+$ T cells, it appears that CD38 expression promotes maintenance and survival of activated T cells. *In vitro*, CD38 limits proliferation of activated T cells, and small interfering RNA targeting of CD38 can increase T cell proliferation (28, 49). In accordance with this, we found that proliferation of adoptively transferred WT P14$^+$ T cells was significantly constrained during Cl13 infection when compared to *Cd38*$^{-/-}$ P14$^+$ T cells at 30 dpi.

While we found that CD38 expression did not alter the development of T cell exhaustion, both Tpex and Tex frequencies and numbers were reduced during Cl13 infection with CD38 deletion. Phenotypically, we observed an increased effector response in *Cd38*$^{-/-}$ P14$^+$ Tpex cells, as shown by more proliferation and granzyme B production. The Tpex population is defined by high expression of the TCF-1 transcription factor and is vital for antiviral and antitumor T cell responses, as Tpex cells are stem-like, able to expand into the Tex population, and can respond to ICB (25, 27). Compared to Tpex cells, Tex cells are more effector-like, having higher cytokine and granzyme B production, as well as increased proliferation (26). In this context, it appears that CD38 may have a cell-intrinsic role in limiting an effector-like Tpex phenotype. However, while CD38 deletion promoted proliferation and KLRG1 expression, the overall frequencies of *Cd38*$^{-/-}$ Tpex and Tex cells were decreased in cotransfer experiments, and Tpex cells lacking CD38 had higher apoptotic frequencies than their WT counterparts. Further, we found that cells expressing CD38 maintained higher TCF-1 frequencies over time, an important factor in Tpex formation. Our data present an interesting paradigm, in which CD38 hinders proliferation and granzyme B production in CD8$^+$ T cells, particularly in the Tpex subset, but also ensures their survival.

Since we saw that CD38 deletion impacted survival of the transferred P14$^+$ T cells during viral infection, we wanted to investigate whether cellular metabolism was also impacted by loss of CD38. The enzymatic activities of CD38 have been reviewed at length (3, 30, 53–55), establishing CD38 as a prominent regulator of cellular NAD$^+$, NAADP, ADPR, and cADPR levels. The consumption of NAD$^+$ by CD38 has the potential to limit T cell metabolism and effector functions, as NAD$^+$ is a key substrate of the immunomodulatory proteins ART, PARP, and SIRT, which are involved in T cell fate, survival, and metabolism (3, 55). *In vitro*, CD38 deletion supports increased oxidative phosphorylation in CD4$^+$ T cells and supports NAD$^+$ levels in cultures of CD8$^+$ T cells (29, 56). Interestingly, our analysis of virus-specific CD8$^+$ T cell metabolism *ex vivo* revealed similar metabolic profiles in WT and *Cd38*$^{-/-}$ P14$^+$ T cells from Arm-infected mice. Given the established NADase activity of CD38, along with previous *in vitro* findings, we anticipated that CD38 deletion would increase the metabolic capabilities of transferred P14$^+$ T cells. To our surprise, we discovered that *Cd38*$^{-/-}$ P14$^+$ T cells from Cl13 infection had reduced oxidative phosphorylation and glycolysis both at basal and maximal conditions. This is opposite of the predicted phenotype arising from NAD$^+$ depletion. However, given that WT and *Cd38*$^{-/-}$ P14$^+$ T cells were transferred into C57BL/6 hosts with functional CD38, along with the recent finding that NAD$^+$ levels are similar in B16-F10 tumors of WT and *Cd38*$^{-/-}$ mice, the impaired metabolism seen in *Cd38*$^{-/-}$ P14$^+$ T cells may be a result of cell-intrinsic CD38 signaling rather than enzymatic activity (29). Additionally, the impact of CD38 on metabolism appears to be correlated with expression levels, as WT P14$^+$ T cells from Arm infection expressed much lower levels of CD38 than those from Cl13 and were spared metabolic impacts upon CD38 deletion. This represents an exciting potential role for CD38 signaling in the mitochondrial fitness of P14$^+$ T cells during Cl13 infection.

Our study shows the regulation of CD38 expression in effector and exhausted CD8$^+$ T cells during viral infection. We found that CD38 is upregulated and expressed at

higher levels on CD8$^+$ T cells in Cl13 than in Arm infection. We showed that CD38 deletion has a cell-intrinsic role in regulating the survival of virus-specific CD8$^+$ T cells throughout the course of viral infection. We found no differences in the metabolism of WT and *Cd38*$^{-/-}$ P14$^+$ T cells from Arm-infected mice, but *Cd38*$^{-/-}$ cells arising during Cl13 infection had decreased oxidative phosphorylation and glycolysis. *Cd38*$^{-/-}$ P14$^+$ Tpex and Tex cells were decreased, and *Cd38*$^{-/-}$ Tpex cells were more proliferative and functional than WT cells, indicating an inhibitory function of CD38 in this cell type. Further, exhausted *Cd38*$^{-/-}$ T cells were decreased in TCF-1$^+$ populations and increased in apoptotic Tpex cells during chronic infection. Our studies show a dual cell-intrinsic role for CD38 in limiting proliferation of virus-specific T cells while also promoting their survival. These data uncover important roles of CD38 in virus-specific T cell responses to infection and highlight new avenues for research into the mechanisms through which CD38 regulates the survival, effector function, and metabolism of exhausted CD8$^+$ T cells.

## MATERIALS AND METHODS

**Mice.** Experimental male C57BL/6J (no. 000664) mice were obtained from The Jackson Laboratory and were used at 6 to 9 weeks of age. B6.129P2-*Cd38*$^{tm1Lnd}$/J (*Cd38*$^{-/-}$, no. 003727) mice were obtained from The Jackson Laboratory and bred for experiments. P14$^+$ mice were obtained from The Scripps Research Institute (originally from Charles D. Surh) and were crossed with *Cd38*$^{-/-}$ mice to obtain P14$^+$ *Cd38*$^{-/-}$ mice. Mice were used at ≥6 weeks of age. Animal care was in accordance with the UC Irvine Institutional Animal Care and Use Committees.

**Virus infection.** Lymphocytic choriomeningitis (LCMV) Armstrong and Cl13 strains were propagated in baby-hamster kidney cells and titrated on Vero African green monkey kidney cells. Frozen stocks were diluted in Vero cell media, and $2 \times 10^5$ PFU of LCMV Armstrong was injected intraperitoneally (i.p.) or $2 \times 10^6$ PFU of LCMV Cl13 was injected intravenously (i.v.). For seahorse metabolism studies, mice were infected with Arm (i.p.) or Cl13 retro-orbitally (r.o.).

**T cell adoptive transfer.** CD8$^+$ T cells were enriched from spleens and lymph nodes (LNs) of WT or *Cd38*$^{-/-}$ P14$^+$ transgenic mice by column-free magnetic negative selection. Single cell suspensions from pooled spleen and LNs were incubated with biotinylated antibodies purchased from BioLegend against CD4 (GK1.5), B220 (RA3-6B2), CD19 (6D5), CD24 (M1/69), CD11b (M1/70), and CD11c (N418). Labeled cells were removed by mixing cell suspension with Streptavidin RapidSpheres (Stemcell Technologies) at room temperature (RT) for 5 min, followed by two 5-min incubations in an EasyEights EasySep Magnet (Stemcell Technologies). Enriched CD8$^+$ T cells were washed in sterile phosphate-buffered saline (PBS) (1×) with fetal bovine serum (FBS) (2%) and purity determined by flow cytometry. For uninfected cotransfer experiments, WT P14$^+$ (CD45.1$^+$) and *Cd38*$^{-/-}$ P14$^+$ (CD45.1$^+$ CD45.2$^+$) T cells normalized (CD8a$^+$ Va2$^+$) and mixed at a 1:1 ratio ($1 \times 10^4$ cells/genotype) and injected retro-orbitally into WT (CD45.2$^+$) recipient mice. Blood, spleen, and LNs were analyzed for adoptively transferred populations 24 h after injection. For infected cotransfer experiments, live WT P14$^+$ (CD45.1$^+$) or *Cd38*$^{-/-}$ P14$^+$ (CD45.1$^+$ CD45.2$^+$) T cells were normalized (CD8a$^+$ Va2$^+$) and mixed at a 1:1 ratio ($1 \times 10^3$ cells/genotype) and injected into WT (CD45.2$^+$) recipient mice i.v. These mice were infected with LCMV 1 day later. Mice were bled r.o., and spleens and lymph nodes were isolated at the indicated time points. Schematic of the cotransfer was created with BioRender (https://www.biorender.com/).

**Flow cytometry.** For cell surface staining, $2 \times 10^6$ cells were incubated with antibodies in staining buffer (PBS, 2% FBS, and 0.01% $NaN_3$) and fixed in PBS with 1.85% formaldehyde for 20 min on ice. For LCMV tetramer staining, cells were incubated with H-2D$^b$-GP$_{33-41}$, H-2D$^b$-GP$_{276-286}$, H-2D$^b$-NP$_{396-404}$, or IA$^b$-$_{66-77}$ tetramers (NIH Core Facility) for 1 h 15 min at room temperature in staining buffer and then fixed with PBS with 1.85% formaldehyde for 20 min on ice. For intracellular cytokine stimulation and staining, cells were resuspended in complete RPMI 1640 (containing 10 mM HEPES, 1% nonessential amino acids and L-glutamine, 1 mM sodium pyruvate, 10% heat-inactivated fetal bovine serum [FBS], and antibiotics) supplemented with 50 U/mL IL-2 (NCI) and 1 mg/mL brefeldin A (BFA) (Sigma) and then incubated with 2 mg/mL LCMV GP$_{33-41}$ peptide (AnaSpec) at 37°C for 4 h. Cells were then fixed and permeabilized using a Cytofix/Cytoperm kit (BD Biosciences) before staining. For intranuclear transcription factor and Ki67 staining, cells were fixed and permeabilized using a Foxp3/transcription factor fixation/permeabilization kit (Fisher) and then stained with anti-human granzyme B (GB12) from Thermo Fisher and Ki67 (B56) from BD Bioscience. Fluorochrome-conjugated antibodies CD44 (IM7), CD45.1 (A20), CD45.2 (104), CD8$\alpha$ (53-6.7), CD4 (RM4-5), CD38 (90), CD160 (7H1), CD223 (C9B7W), CD279 (RMP1-30), CD366 (RMT3-23), CD244.2 (m2B4 [B6] 458.1), KLRG1 (2FI/KLRG1), and CD69 (H1.2F3) were purchased from BioLegend. Fluorochrome-conjugated Ly-108 (13G3) was purchased from BD Biosciences. Fluorochrome-conjugated TCF-1 (C63D9) was purchased from Cell Signaling Technology. Surface stains were performed at a 1:200 dilution, while intracellular and intranuclear stains were performed at a 1:100 dilution. Caspase-3 staining was done using PI (Sigma-Aldrich) and CaspGLOW fluorescein active caspase-3 staining kit (Thermo Fisher) and following manufacturer's instructions. All data were collected on a NovoCyte 3000 (Agilent) and analyzed using FlowJo Software (Tree Star).

**Seahorse assay.** Cotransferred WT or *Cd38*$^{-/-}$ P14$^+$ T cells were isolated from spleens of host mice at 8 days post Armstrong or Cl13 infection. CD8$^+$ T cells were purified by negative selection (see

methods in "T cell adoptive transfer"); stained for 10 min with propidium iodide (PI) in complete media RPMI 1640 (containing 10 mM HEPES, 1% nonessential amino acids and L-glutamine, 1 mM sodium pyruvate, 10% heat inactivated FBS, and 1% antibiotics [penicillin, streptomycin, L-glutamine] from Corning); surface stained with CD8 BV785 (53-6.7), CD45.1 PB (A20), and CD45.2 fluorescein isothiocyanate (FITC) (104) from BioLegend; and sorted on a BD FACSAria Fusion at >95% purity. Fluorescence-activated cell sorting (FACS) was used to isolate WT P14$^+$ (PI$^-$ CD8$^+$ CD45.1$^+$ CD45.2$^-$) and *Cd38*$^{-/-}$ P14$^+$ (PI$^-$ CD8$^+$ CD45.1$^+$ CD45.2$^+$) T cells. Live cells were counted immediately after sorting and adhered onto the wells of a poly-D-lysine coated XF96 plate at between 500,000 and 550,000 cells/well (exact counts were noted and used for normalization). The Seahorse XF Mito stress test was performed to measure OCR and ECAR of cells plated in XF media (nonbuffered Dulbecco modified Eagle medium [DMEM] containing 10 mM glucose, 4 mM L-glutamine, and 2 mM sodium pyruvate) under basal conditions and in response to 1 $\mu$M oligomycin (Calbiochem), 1.5 $\mu$M fluoro-carbonyl cyanide phenylhydrazone (FCCP) (Enzo), and 1 $\mu$M rotenone + 1 $\mu$M antimycin A (Enzo) with the XF96 extracellular flux analyzer (Seahorse Bioscience). Data were normalized using Wave software (Agilent). Basal respiration values were determined as the mean OCR of the last 3 baseline data points minus the median of the 3 OCR data points after antimycin A and rotenone addition (57). Maximal OCR values were determined as the maximum of the three OCR values after FCCP addition minus the median of the last 3 values after rotenone and antimycin A addition. Basal ECAR values were determined as the mean of the last 3 baseline points. Maximal ECAR values were determined as the highest ECAR point after addition of FCCP. Basal OCR/ECAR was determined as the mean OCR of the last 3 baseline data points divided by the mean of the ECAR of the last 3 baseline data points. Maximal OCR/ECAR was determined as the highest of the 3 OCR values after the addition of FCCP divided by the corresponding ECAR value.

**Quantification and statistical analysis.** Flow cytometry data were analyzed with FlowJo software (TreeStar). Graphs of flow cytometry data and Seahorse data were prepared with GraphPad Prism software. GraphPad Prism was used for statistical analysis to compare outcomes using a two-tailed unpaired Student's *t* test, Mann-Whitney, or a two-tailed paired *t* test where indicated; significance was set to $P \leq 0.05$ and represented as follows: *, $P \leq 0.05$; **, $P \leq 0.01$; ***, $P \leq 0.001$; and ****, $P \leq 0.0001$. Error bars show standard error of the mean (SEM).

## SUPPLEMENTAL MATERIAL

Supplemental material is available online only.

**SUPPLEMENTAL FILE 1**, PDF file, 1.3 MB.

## ACKNOWLEDGMENTS

We thank all current and former members in the Tinoco Laboratory for all their constructive comments and advice during this project.

This work was supported by the NIH (R01 AI137239 to R. Tinoco and R00 HD098330 to D. A. Nicholas), T32 Training Program for Interdisciplinary Cancer Research IDCR (T32CA009054 to J. M. DeRogatis), T32 virus-host interactions: a multi-scale training program (T32AI007319 to E. N. Neubert), and T32 Microbiology and Infectious Diseases training grant (T32AI141346 to K. M. Viramontes). Graduate Assistance in Areas of National Need (GAANN) fellowship (P200A210024 to J.M. DeRogatis).

We thank Jie Wu (UCI Genomics High Throughput Facility) for human HCV RNAseq analysis, which is a Chao Family Comprehensive Cancer Center (CFCCC) shared resource supported by the Cancer Center Support Grant (P30CA062203). We thank Jennifer Atwood at the UCI Institute for Immunology Flow Core, a shared resource of the Cancer Center Support Grant (CA-62203) at the University of California, Irvine, for assistance with FACS. This study was also supported by the UCI Stem Cell Research Center with additional support from California Institute for Regenerative Medicine grant CL1-00520-1.2 to Vanessa Scarfone and the UC Irvine Stem Cell FACS Core.

We report no disclosures.

R. Tinoco conceived, directed, and obtained funding for the project. J. M. DeRogatis and R. Tinoco conceptualized, designed, and analyzed the experiments and wrote the manuscript. J. M. DeRogatis, E. N. Neubert, K. M. Viramontes, and M. L. Henriquez performed the experiments. J. M. DeRogatis, D. A. Nicholas, and R. Tinoco designed, analyzed, and interpreted metabolism studies. All authors provided feedback and approved the manuscript.

## REFERENCES

1. Malavasi F, Deaglio S, Funaro A, Ferrero E, Horenstein AL, Ortolan E, Vaisitti T, Aydin S. 2008. Evolution and function of the ADP ribosyl cyclase/CD38 gene family in physiology and pathology. Physiol Rev 88:841–886. https://doi.org/10.1152/physrev.00035.2007.

2. Munoz P, Mittelbrunn M, de la Fuente H, Perez-Martinez M, Garcia-Perez A, Ariza-Veguillas A, Malavasi F, Zubiaur M, Sanchez-Madrid F, Sancho J. 2008. Antigen-induced clustering of surface CD38 and recruitment of intracellular CD38 to the immunologic synapse. Blood 111:3653–3664. https://doi.org/10.1182/blood-2007-07-101600.
3. Kar A, Mehrotra S, Chatterjee S. 2020. CD38: T cell immuno-metabolic modulator. Cells 9:1716. https://doi.org/10.3390/cells9071716.
4. Canto C, Menzies KJ, Auwerx J. 2015. NAD(+) metabolism and the control of energy homeostasis: a balancing act between mitochondria and the nucleus. Cell Metab 22:31–53. https://doi.org/10.1016/j.cmet.2015.05.023.
5. Aarhus R, Graeff RM, Dickey DM, Walseth TF, Lee HC. 1995. ADP-ribosyl cyclase and CD38 catalyze the synthesis of a calcium-mobilizing metabolite from NADP. J Biol Chem 270:30327–30333. https://doi.org/10.1074/jbc.270.51.30327.
6. Gelman L, Deterre P, Gouy H, Boumsell L, Debre P, Bismuth G. 1993. The lymphocyte surface antigen CD38 acts as a nicotinamide adenine dinucleotide glycohydrolase in human T lymphocytes. Eur J Immunol 23:3361–3364. https://doi.org/10.1002/eji.1830231245.
7. Zubiaur M, Izquierdo M, Terhorst C, Malavasi F, Sancho J. 1997. CD38 ligation results in activation of the Raf-1/mitogen-activated protein kinase and the CD3-zeta/zeta-associated protein-70 signaling pathways in Jurkat T lymphocytes. J Immunol 159:193–205. https://doi.org/10.4049/jimmunol.159.1.193.
8. Radziewicz H, Ibegbu CC, Hon H, Osborn MK, Obideen K, Wehbi M, Freeman GJ, Lennox JL, Workowski KA, Hanson HL, Grakoui A. 2008. Impaired hepatitis C virus (HCV)-specific effector CD8+ T cells undergo massive apoptosis in the peripheral blood during acute HCV infection and in the liver during the chronic phase of infection. J Virol 82:9808–9822. https://doi.org/10.1128/JVI.01075-08.
9. Hua S, Lecuroux C, Saez-Cirion A, Pancino G, Girault I, Versmisse P, Boufassa F, Taulera O, Sinet M, Lambotte O, Venet A. 2014. Potential role for HIV-specific CD38$^-$/HLA-DR$^+$CD8$^+$ T cells in viral suppression and cytotoxicity in HIV controllers. PLoS One 9:e101920. https://doi.org/10.1371/journal.pone.0101920.
10. Murray SM, Down CM, Boulware DR, Stauffer WM, Cavert WP, Schacker TW, Brenchley JM, Douek DC. 2010. Reduction of immune activation with chloroquine therapy during chronic HIV infection. J Virol 84:12082–12086. https://doi.org/10.1128/JVI.01466-10.
11. Chandele A, Sewatanon J, Gunisetty S, Singla M, Onlamoon N, Akondy RS, Kissick HT, Nayak K, Reddy ES, Kalam H, Kumar D, Verma A, Panda H, Wang S, Angkasekwinai N, Pattanapanyasat K, Chokephaibulkit K, Medigeshi GR, Lodha R, Kabra S, Ahmed R, Murali-Krishna K. 2016. Characterization of human CD8 T cell responses in Dengue virus-infected patients from India. J Virol 90:11259–11278. https://doi.org/10.1128/JVI.01424-16.
12. Fox A, Le NM, Horby P, van Doorn HR, Nguyen VT, Nguyen HH, Nguyen TC, Vu DP, Nguyen MH, Diep NT, Bich VT, Huong HT, Taylor WR, Farrar J, Wertheim H, Nguyen VK. 2012. Severe pandemic H1N1 2009 infection is associated with transient NK and T deficiency and aberrant CD8 responses. PLoS One 7:e31535. https://doi.org/10.1371/journal.pone.0031535.
13. Wang Z, Zhu L, Nguyen THO, Wan Y, Sant S, Quinones-Parra SM, Crawford JC, Eltahla AA, Rizzetto S, Bull RA, Qiu C, Koutsakos M, Clemens EB, Loh L, Chen T, Liu L, Cao P, Ren Y, Kedzierski L, Kotsimbos T, McCaw JM, La Gruta NL, Turner SJ, Cheng AC, Luciani F, Zhang X, Doherty PC, Thomas PG, Xu J, Kedzierska K. 2018. Clonally diverse CD38(+)HLA-DR(+)CD8(+) T cells persist during fatal H7N9 disease. Nat Commun 9:824. https://doi.org/10.1038/s41467-018-03243-7.
14. Thevarajan I, Nguyen THO, Koutsakos M, Druce J, Caly L, van de Sandt CE, Jia X, Nicholson S, Catton M, Cowie B, Tong SYC, Lewin SR, Kedzierska K. 2020. Breadth of concomitant immune responses prior to patient recovery: a case report of non-severe COVID-19. Nat Med 26:453–455. https://doi.org/10.1038/s41591-020-0819-2.
15. Ruibal P, Oestereich L, Ludtke A, Becker-Ziaja B, Wozniak DM, Kerber R, Korva M, Cabeza-Cabrerizo M, Bore JA, Koundouno FR, Duraffour S, Weller R, Thorenz A, Cimini E, Viola D, Agrati C, Repits J, Afrough B, Cowley LA, Ngabo D, Hinzmann J, Mertens M, Vitoriano I, Logue CH, Boettcher JP, Pallasch E, Sachse A, Bah A, Nitzsche K, Kuisma E, Michel J, Holm T, Zekeng EG, Garcia-Dorival I, Wolfel R, Stoecker K, Fleischmann E, Strecker T, Di Caro A, Avsic-Zupanc T, Kurth A, Meschi S, Mely S, Newman E, Bocquin A, Kis Z, Kelterbaum A, Molkenthin P, Carletti F, Portmann J, et al. 2016. Unique human immune signature of Ebola virus disease in Guinea. Nature 533:100–104. https://doi.org/10.1038/nature17949.
16. Jia X, Chua BY, Loh L, Koutsakos M, Kedzierski L, Olshansky M, Heath WR, Chang SY, Xu J, Wang Z, Kedzierska K. 2021. High expression of CD38 and MHC class II on CD8(+) T cells during severe influenza disease reflects bystander activation and trogocytosis. Clin Transl Immunology 10:e1336. https://doi.org/10.1002/cti2.1336.
17. Horenstein AL, Chillemi A, Zaccarello G, Bruzzone S, Quarona V, Zito A, Serra S, Malavasi F. 2013. A CD38/CD203a/CD73 ectoenzymatic pathway independent of CD39 drives a novel adenosinergic loop in human T lymphocytes. Oncoimmunology 2:e26246. https://doi.org/10.4161/onci.26246.
18. Allard B, Beavis PA, Darcy PK, Stagg J. 2016. Immunosuppressive activities of adenosine in cancer. Curr Opin Pharmacol 29:7–16. https://doi.org/10.1016/j.coph.2016.04.001.
19. Ohta A, Gorelik E, Prasad SJ, Ronchese F, Lukashev D, Wong MK, Huang X, Caldwell S, Liu K, Smith P, Chen JF, Jackson EK, Apasov S, Abrams S, Sitkovsky M. 2006. A2A adenosine receptor protects tumors from antitumor T cells. Proc Natl Acad Sci U S A 103:13132–13137. https://doi.org/10.1073/pnas.0605251103.
20. Chen L, Diao L, Yang Y, Yi X, Rodriguez BL, Li Y, Villalobos PA, Cascone T, Liu X, Tan L, Lorenzi PL, Huang A, Zhao Q, Peng D, Fradette JJ, Peng DH, Ungewiss C, Roybal J, Tong P, Oba J, Skoulidis F, Peng W, Carter BW, Gay CM, Fan Y, Class CA, Zhu J, Rodriguez-Canales J, Kawakami M, Byers LA, Woodman SE, Papadimitrakopoulou VA, Dmitrovsky E, Wang J, Ullrich SE, Wistuba II, Heymach JV, Qin FX, Gibbons DL. 2018. CD38-mediated immunosuppression as a mechanism of tumor cell escape from PD-1/PD-L1 blockade. Cancer Discov 8:1156–1175. https://doi.org/10.1158/2159-8290.CD-17-1033.
21. Beavis PA, Milenkovski N, Henderson MA, John LB, Allard B, Loi S, Kershaw MH, Stagg J, Darcy PK. 2015. Adenosine receptor 2A blockade increases the efficacy of anti-PD-1 through enhanced antitumor T-cell responses. Cancer Immunol Res 3:506–517. https://doi.org/10.1158/2326-6066.CIR-14-0211.
22. Philip M, Fairchild L, Sun L, Horste EL, Camara S, Shakiba M, Scott AC, Viale A, Lauer P, Merghoub T, Hellmann MD, Wolchok JD, Leslie CS, Schietinger A. 2017. Chromatin states define tumour-specific T cell dysfunction and reprogramming. Nature 545:452–456. https://doi.org/10.1038/nature22367.
23. Moskophidis D, Lechner F, Pircher H, Zinkernagel RM. 1993. Virus persistence in acutely infected immunocompetent mice by exhaustion of antiviral cytotoxic effector T cells. Nature 362:758–761. https://doi.org/10.1038/362758a0.
24. Speiser DE, Utzschneider DT, Oberle SG, Munz C, Romero P, Zehn D. 2014. T cell differentiation in chronic infection and cancer: functional adaptation or exhaustion? Nat Rev Immunol 14:768–774. https://doi.org/10.1038/nri3740.
25. Im SJ, Hashimoto M, Gerner MY, Lee J, Kissick HT, Burger MC, Shan Q, Hale JS, Lee J, Nasti TH, Sharpe AH, Freeman GJ, Germain RN, Nakaya HI, Xue HH, Ahmed R. 2016. Defining CD8+ T cells that provide the proliferative burst after PD-1 therapy. Nature 537:417–421. https://doi.org/10.1038/nature19330.
26. Miller BC, Sen DR, Al Abosy R, Bi K, Virkud YV, LaFleur MW, Yates KB, Lako A, Felt K, Naik GS, Manos M, Gjini E, Kuchroo JR, Ishizuka JJ, Collier JL, Griffin GK, Maleri S, Comstock DE, Weiss SA, Brown FD, Panda A, Zimmer MD, Manguso RT, Hodi FS, Rodig SJ, Sharpe AH, Haining WN. 2019. Subsets of exhausted CD8(+) T cells differentially mediate tumor control and respond to checkpoint blockade. Nat Immunol 20:326–336. https://doi.org/10.1038/s41590-019-0312-6.
27. Utzschneider DT, Gabriel SS, Chisanga D, Gloury R, Gubser PM, Vasanthakumar A, Shi W, Kallies A. 2020. Early precursor T cells establish and propagate T cell exhaustion in chronic infection. Nat Immunol 21:1256–1266. https://doi.org/10.1038/s41590-020-0760-z.
28. Verma V, Shrimali RK, Ahmad S, Dai W, Wang H, Lu S, Nandre R, Gaur P, Lopez J, Sade-Feldman M, Yizhak K, Bjorgaard SL, Flaherty KT, Wargo JA, Boland GM, Sullivan RJ, Getz G, Hammond SA, Tan M, Qi J, Wong P, Merghoub T, Wolchok J, Hacohen N, Janik JE, Mkrtichyan M, Gupta S, Khleif SN. 2019. PD-1 blockade in subprimed CD8 cells induces dysfunctional PD-1(+)CD38(hi) cells and anti-PD-1 resistance. Nat Immunol 20:1231–1243. https://doi.org/10.1038/s41590-019-0441-y.
29. Ma K, Sun L, Shen M, Zhang X, Xiao Z, Wang J, Liu X, Jiang K, Xiao-Feng Qin F, Guo F, Zhang B, Zhang L. 2022. Functional assessment of the cell-autonomous role of NADase CD38 in regulating CD8(+) T cell exhaustion. iScience 25:104347. https://doi.org/10.1016/j.isci.2022.104347.
30. Glaria E, Valledor AF. 2020. Roles of CD38 in the immune response to infection. Cells 9:228. https://doi.org/10.3390/cells9010228.
31. Liu Z, Hultin LE, Cumberland WG, Hultin P, Schmid I, Matud JL, Detels R, Giorgi JV. 1996. Elevated relative fluorescence intensity of CD38 antigen expression on CD8+ T cells is a marker of poor prognosis in HIV infection: results of 6 years of follow-up. Cytometry 26:1–7. https://doi.org/10.1002/(SICI)1097-0320(19960315)26:1%3C1::AID-CYTO1%3E3.0.CO;2-L.

32. Mocroft A, Bofill M, Lipman M, Medina E, Borthwick N, Timms A, Batista L, Winter M, Sabin CA, Johnson M, Lee CA, Phillips A, Janossy G. 1997. CD8+, CD38+ lymphocyte percent: a useful immunological marker for monitoring HIV-1-infected patients. J Acquir Immune Defic Syndr Hum Retrovirol 14:158–162. https://doi.org/10.1097/00042560-199702010-00009.
33. Burgisser P, Hammann C, Kaufmann D, Battegay M, Rutschmann OT. 1999. Expression of CD28 and CD38 by CD8+ T lymphocytes in HIV-1 infection correlates with markers of disease severity and changes towards normalization under treatment. The Swiss HIV Cohort study. Clin Exp Immunol 115:458–463. https://doi.org/10.1046/j.1365-2249.1999.00818.x.
34. Hensel N, Gu Z, Sagar, Wieland D, Jechow K, Kemming J, Llewellyn-Lacey S, Gostick E, Sogukpinar O, Emmerich F, Price DA, Bengsch B, Boettler T, Neumann-Haefelin C, Eils R, Conrad C, Bartenschlager R, Grun D, Ishaque N, Thimme R, Hofmann M. 2021. Memory-like HCV-specific CD8(+) T cells retain a molecular scar after cure of chronic HCV infection. Nat Immunol 22:229–239.
35. Timperi E, Barnaba V. 2021. CD39 regulation and functions in T cells. Int J Mol Sci 22:8068. https://doi.org/10.3390/ijms22158068.
36. Dolina JS, Van Braeckel-Budimir N, Thomas GD, Salek-Ardakani S. 2021. CD8(+) T cell exhaustion in cancer. Front Immunol 12:715234. https://doi.org/10.3389/fimmu.2021.715234.
37. Chen PM, Katsuyama E, Satyam A, Li H, Rubio J, Jung S, Andrzejewski S, Becherer JD, Tsokos MG, Abdi R, Tsokos GC. 2022. CD38 reduces mitochondrial fitness and cytotoxic T cell response against viral infection in lupus patients by suppressing mitophagy. Sci Adv 8:eabo4271. https://doi.org/10.1126/sciadv.abo4271.
38. Ndhlovu ZM, Kamya P, Mewalal N, Kloverpris HN, Nkosi T, Pretorius K, Laher F, Ogunshola F, Chopera D, Shekhar K, Ghebremichael M, Ismail N, Moodley A, Malik A, Leslie A, Goulder PJ, Buus S, Chakraborty A, Dong K, Ndung'u T, Walker BD. 2015. Magnitude and kinetics of CD8+ T cell activation during hyperacute HIV infection impact viral set point. Immunity 43:591–604. https://doi.org/10.1016/j.immuni.2015.08.012.
39. Vigano A, Saresella M, Villa ML, Ferrante P, Clerici M. 2000. CD38+CD8+ T cells as a marker of poor response to therapy in HIV-infected individuals. Chem Immunol 75:207–217. https://doi.org/10.1159/000058770.
40. McElroy AK, Akondy RS, Davis CW, Ellebedy AH, Mehta AK, Kraft CS, Lyon GM, Ribner BS, Varkey J, Sidney J, Sette A, Campbell S, Stroher U, Damon I, Nichol ST, Spiropoulou CF, Ahmed R. 2015. Human Ebola virus infection results in substantial immune activation. Proc Natl Acad Sci U S A 112:4719–4724. https://doi.org/10.1073/pnas.1502619112.
41. Sen DR, Kaminski J, Barnitz RA, Kurachi M, Gerdemann U, Yates KB, Tsao HW, Godec J, LaFleur MW, Brown FD, Tonnerre P, Chung RT, Tully DC, Allen TM, Frahm N, Lauer GM, Wherry EJ, Yosef N, Haining WN. 2016. The epigenetic landscape of T cell exhaustion. Science 354:1165–1169. https://doi.org/10.1126/science.aae0491.
42. Scott-Browne JP, Lopez-Moyado IF, Trifari S, Wong V, Chavez L, Rao A, Pereira RM. 2016. Dynamic changes in chromatin accessibility occur in CD8 (+) T cells responding to viral infection. Immunity 45:1327–1340. https://doi.org/10.1016/j.immuni.2016.10.028.
43. Beltra JC, Manne S, Abdel-Hakeem MS, Kurachi M, Giles JR, Chen Z, Casella V, Ngiow SF, Khan O, Huang YJ, Yan P, Nzingha K, Xu W, Amaravadi RK, Xu X, Karakousis GC, Mitchell TC, Schuchter LM, Huang AC, Wherry EJ. 2020. Developmental relationships of four exhausted CD8(+) T cell subsets reveals underlying transcriptional and epigenetic landscape control mechanisms. Immunity 52:825–841. https://doi.org/10.1016/j.immuni.2020.04.014.
44. Karakasheva TA, Waldron TJ, Eruslanov E, Kim SB, Lee JS, O'Brien S, Hicks PD, Basu D, Singhal S, Malavasi F, Rustgi AK. 2015. CD38-expressing myeloid-derived suppressor cells promote tumor growth in a murine model of esophageal cancer. Cancer Res 75:4074–4085. https://doi.org/10.1158/0008-5472.CAN-14-3639.
45. Morandi F, Morandi B, Horenstein AL, Chillemi A, Quarona V, Zaccarello G, Carrega P, Ferlazzo G, Mingari MC, Moretta L, Pistoia V, Malavasi F. 2015. A non-canonical adenosinergic pathway led by CD38 in human melanoma cells induces suppression of T cell proliferation. Oncotarget 6:25602–25618. https://doi.org/10.18632/oncotarget.4693.
46. Perrot I, Michaud HA, Giraudon-Paoli M, Augier S, Docquier A, Gros L, Courtois R, Dejou C, Jecko D, Becquart O, Rispaud-Blanc H, Gauthier L, Rossi B, Chanteux S, Gourdin N, Amigues B, Roussel A, Bensussan A, Eliaou JF, Bastid J, Romagne F, Morel Y, Narni-Mancinelli E, Vivier E, Paturel C, Bonnefoy N. 2019. Blocking antibodies targeting the CD39/CD73 immunosuppressive pathway unleash immune responses in combination cancer therapies. Cell Rep 27:2411–2425. https://doi.org/10.1016/j.celrep.2019.04.091.
47. Deaglio S, Robson SC. 2011. Ectonucleotidases as regulators of purinergic signaling in thrombosis, inflammation, and immunity. Adv Pharmacol 61:301–332. https://doi.org/10.1016/B978-0-12-385526-8.00010-2.
48. Antonioli L, Pacher P, Vizi ES, Hasko G. 2013. CD39 and CD73 in immunity and inflammation. Trends Mol Med 19:355–367. https://doi.org/10.1016/j.molmed.2013.03.005.
49. Sandoval-Montes C, Santos-Argumedo L. 2005. CD38 is expressed selectively during the activation of a subset of mature T cells with reduced proliferation but improved potential to produce cytokines. J Leukoc Biol 77:513–521. https://doi.org/10.1189/jlb.0404262.
50. Bahri R, Bollinger A, Bollinger T, Orinska Z, Bulfone-Paus S. 2012. Ectonucleotidase CD38 demarcates regulatory, memory-like CD8+ T cells with IFN-gamma-mediated suppressor activities. PLoS One 7:e45234. https://doi.org/10.1371/journal.pone.0045234.
51. Ostendorf L, Burns M, Durek P, Heinz GA, Heinrich F, Garantziotis P, Enghard P, Richter U, Biesen R, Schneider U, Knebel F, Burmester G, Radbruch A, Mei HE, Mashreghi MF, Hiepe F, Alexander T. 2020. Targeting CD38 with daratumumab in refractory systemic lupus erythematosus. N Engl J Med 383:1149–1155. https://doi.org/10.1056/NEJMoa2023325.
52. Callan MF, Tan L, Annels N, Ogg GS, Wilson JD, O'Callaghan CA, Steven N, McMichael AJ, Rickinson AB. 1998. Direct visualization of antigen-specific CD8+ T cells during the primary immune response to Epstein-Barr virus in vivo. J Exp Med 187:1395–1402. https://doi.org/10.1084/jem.187.9.1395.
53. Piedra-Quintero ZL, Wilson Z, Nava P, Guerau-de-Arellano M. 2020. CD38: an immunomodulatory molecule in inflammation and autoimmunity. Front Immunol 11:597959. https://doi.org/10.3389/fimmu.2020.597959.
54. Morandi F, Horenstein AL, Malavasi F. 2021. The key role of NAD(+) in anti-tumor immune response: an update. Front Immunol 12:658263. https://doi.org/10.3389/fimmu.2021.658263.
55. Li W, Liang L, Liao Q, Li Y, Zhou Y. 2022. CD38: an important regulator of T cell function. Biomed Pharmacother 153:113395. https://doi.org/10.1016/j.biopha.2022.113395.
56. Chatterjee S, Daenthanasanmak A, Chakraborty P, Wyatt MW, Dhar P, Selvam SP, Fu J, Zhang J, Nguyen H, Kang I, Toth K, Al-Homrani M, Husain M, Beeson G, Ball L, Helke K, Husain S, Garrett-Mayer E, Hardiman G, Mehrotra M, Nishimura MI, Beeson CC, Bupp MG, Wu J, Ogretmen B, Paulos CM, Rathmell J, Yu XZ, Mehrotra S. 2018. CD38-NAD(+) axis regulates immunotherapeutic anti-tumor T cell response. Cell Metab 27:85–100. https://doi.org/10.1016/j.cmet.2017.10.006.
57. Nicholas D, Proctor EA, Raval FM, Ip BC, Habib C, Ritou E, Grammatopoulos TN, Steenkamp D, Dooms H, Apovian CM, Lauffenburger DA, Nikolajczyk BS. 2017. Advances in the quantification of mitochondrial function in primary human immune cells through extracellular flux analysis. PLoS One 12:e0170975. https://doi.org/10.1371/journal.pone.0170975.